공학박사 학위논문

Charge Enhanced Epitaxial Growth, Film Dewetting and Sheet Metal Recrystallization

하전에 의한 단결정 박막성장, 금속박막의 디웨팅 및 금속시트의 재결정 향상

2020 년 2 월

서울대학교 대학원

재료공학부

박 순 원

Charge Enhanced Epitaxial Growth, Film Dewetting and Sheet Metal Recrystallization

지도교수 황 농 문

이 논문을 공학박사 학위논문으로 제출함
2020 년 2 월

서울대학교 대학원
재료공학부
박 순 원

박순원의 공학박사 학위논문을 인준함
2020 년 2 월

위 원 장 박 은 수 (인)

부위원장 황 농 문 (인)

위 원 장 호 원 (인)

위 원 나 태 욱 (인)

위 원 정 재 수 (인)

Abstract

Charge Enhanced Epitaxial Growth, Film Dewetting and Sheet Metal Recrystallization

Soon-Won Park

Department of Materials Science and Engineering

The Graduate School

Seoul National University

There are increasing evidences that charges should make nanoparticles liquid-like or enhance diffusion in nanoparticles. Considering this, the deposition behavior of silicon films by radio frequency plasma enhanced chemical vapor deposition (RF-PECVD) was studied by the non-classical crystallization, where the building block of deposition is charged nanoparticles generated in the gas phase of the reactor.

To examine the effect of the bias on the epitaxial growth, films were deposited on the silicon wafer substrate under the condition of

the biases of 0 V, +1000 V and －1000 V applied to the substrate holder. A fully epitaxial film could be grown on a silicon wafer at 550 ℃ under the bias of －1000 V. In order to confirm the existence of nanoparticles in the RF-PECVD reactor, nanoparticles were captured on the membrane of the transmission electron microscope (TEM) grid under the condition of the DC bias applied to the holder. The capturing behavior of nanoparticles depended on the bias and the conductivity of the membrane.

Also, two series of experiments were made to clarify whether plasma enhanced kinetics come from ion bombardments or from the charge buildup. One is the comparison of dewetting kinetics of Au and Sn films in the inductively-coupled plasma between floating and grounded states. The other is the comparison of recrystallization kinetics of the Fe-1%Si and pure Cu sheet sample in the inductively-coupled plasma between floating and grounded states. Both dewetting and recrystallization kinetics were much more enhanced in the floating state than in the grounded state. These results show that the charge buildup is responsible for the plasma enhanced kinetics.

keywords : Non-classical crystallization; charge; liquid-like property; silicon thin film deposition; dewetting; recrystallization

Student Number : 2014-22517

Contents

List of figures

part, and (c) HRTEM image of the interfacial region.

[Fig. 2.4] TEM cross-section images of the silicon films on (100) silicon wafer with -1000 V: (a) low magnification TEM image of films, (b) HRTEM image of the silicon film at middle part, and (c) HRTEM image of the interfacial region between silicon wafer and silicon film.

[Fig. 2.5] TEM images of silicon nanoparticles captured on SiO TEM grid with an exposure time of 15 sec for (a) 0 V, (b) +1000 V, and (c) -1000 V.

[Fig. 2.6] HRTEM images of silicon nanoparticles captured on SiO TEM grid with an exposure time of 15 sec for (a) 0 V, (b) +1000 V, and (c) -1000 V.

[Fig. 2.7] TEM images of silicon nanoparticles captured on carbon TEM grid with an exposure time of 15 sec for (a) 0 V, (b) +1000 V, and (c) -1000 V.

[Fig. 2.8] HRTEM images of silicon nanoparticles captured on carbon TEM grid with an exposure time of 15 sec for (a) 0 V, (b) +1000 V, and (c) -1000 V.

[Fig. 2.9] The growth rate of silicon films prepared with various substrates at 400 ℃ and bias for 15 min.

elongated silicon substrate. Above are FESEM images of the elongated Sn film grounded by an Al tape after H_2 plasma treatment for 2 min. (b) the area closest to the conducting Al tape, (c) the area at the middle, and (d) the area farthest from the conducting Al tape.

[Fig. 3.7] (a) A schematic of the experiment to induce the charge building up by applying DC bias to the sample, which is heated 300 ℃ and held for 2 h. Above are FESEM images of (b) the sample applied by -8500 V and (c) the sample without bias.

[Fig. 4.1] Schematic of the inductively coupled plasma (ICP) chamber.

[Fig. 4.2] OM cross section images of Fe-1%Si samples (a) as-cold rolled, (b) thermally annealed at 600 °C for 120 min, (c) thermally annealed 500 °C for 120 min and (d) thermally and plasma annealed at 500 °C for 120 min.

[Fig. 4.3] (a) OM cross section and (b) EBSD images of floating Fe-1%Si sample heated for 120 min at 400 °C and exposed to plasma of 700 W, and (c) OM cross section and (d) EBSD images of grounded Fe-1%Si under the same condition. (e) Average grain size of the floating Fe-1%Si sample heated for 120 min at 400 °C and exposed to plasma of 700 W, and (f) Average grain size of the grounded Fe-1%Si under the same

condition.

[Fig. 4.4] EBSD images showing the recrystallization fraction of (a) floating and (b) grounded Fe-1%Si samples heated at 400 °C and exposed to plasma of 700 W.

[Fig. 4.5] (a) OM cross section and (b) EBSD images of floating Fe-1%Si sample heated for 120 min at 450 °C and exposed to plasma of 650 W and (c) OM cross section and (d) EBSD images of grounded Fe-1%Si sample heated for 120 min at 450 °C and exposed to plasma of 650 W. (e) Average grain size of the floating Fe-1%Si sample heated for 120 min at 450 °C and exposed to plasma of 650 W, and (f) Average grain size of the grounded Fe-1%Si under the same condition.

[Fig. 4.6] EBSD images of (a) floating pure Cu sheet sample exposed to plasma of 250 W for 120 min, and (b) grounded pure Cu under the same condition. (c) Average grain size of floating pure Cu sheet sample exposed to plasma of 250 W for 120 min, and (d) Average grain size of grounded pure Cu under the same condition.

Chapter 1.

1. Introduction

1.1 Non-classical crystallization

Recently, non-classical crystallization, where the building block of crystal growth is neither an atom nor a molecule but a nanoparticle, has been extensively studied in solution[1-4] and in the gas phase[5-7]. Non-classical crystallization has now become so established that several review papers[8, 9] and a few books[10, 11] have been published. Moreover, tutorial or technical sessions devoted to this topic began to be included in the international conference.

Nonetheless, there are many phenomena in the non-classical crystallization that are not understood clearly. One puzzling phenomenon among them is the formation of void-free grains or crystals, which are much larger than the size of an individual building block. One explanation suggested by Banfield[12] is the orientation attachment, where the building block rotates or aligns into the same orientation as that of the crystal just before joining into it.

Another explanation suggested by Hwang[13-15] is the presence of charge in the nanoparticle. According to Hwang[16-19], the crystallization behavior changes drastically depending on whether the building block is charged or not. Neutral building blocks or nanoparticles would produce the highly porous skeletal structure whereas charged ones would produce dense films or nanostructures. For example, charged diamond nanoparticles in the gas phase produce a porous soot structure on the grounded Fe substrate but produce

diamond crystals on initially formed soot on the floating Fe substrate[20].(Fig. 1.1)

Also, Yoon et al.[21, 22] compared the deposition behavior between floating and grounded silicon substrates under the condition where abundant charged silicon nanoparticles were generated in the atmospheric silicon chemical vapor deposition (CVD) process. At the N_2 flow rate of 500 standard cubic centimeter per minute (sccm), single crystalline silicon nanowires were grown on the floating substrate where as silicon nanoparticles were formed on the grounded substrate.(Fig. 1.2) At the N_2 flow rate of 1000 sccm, a dense silicon film was deposited on the floating substrate where as rather a porous silicon film was deposited on the grounded substrate.(Fig. 1.3)

On the other hand, in the plasma enhanced CVD (PECVD) process, a concept similar to non-classical crystallization was suggested by Cabarrocas[23], Vladimirov and Ostrikov[24], and Nunomura et al.[25]. Cabarrocas et al.[26-29] called such a nanoparticle-incorporated silicon film a polymorphous film, which refers to amorphous Si (a-Si:H) matrix embedded with silicon nanocrystallites. Ostrikov[30-33] made an extensive review on the incorporation of gas-phase nuclei into nanostructures for a reactive-plasma assisted nano-assembly process[25, 34-36]. Shiratani and his colleagues [26, 35-37] measured the size distribution of nanoparticles generated in the gas phase under various conditions of PECVD using the time evolution of a laser light scattering (LLS) intensity.

1.2 Details of study

In this thesis, the deposition behavior of charged nanoparticles generated in the gas phase will be examined during the radio frequency plasma enhanced chemical vapor deposition (RF-PECVD). Especially, the effect of the bias applied to the substrate holder on the deposition behavior will be studied focusing on the epitaxial growth on the silicon wafer substrate. And the dewetting behavior of Au and Sn films, which were exposed to inductively-coupled plasma, was compared between floating and grounded states. To extend this study further, the plasma enhanced recrystallization kinetics of the Fe-1%Si sheet sample was compared between floating and grounded states.

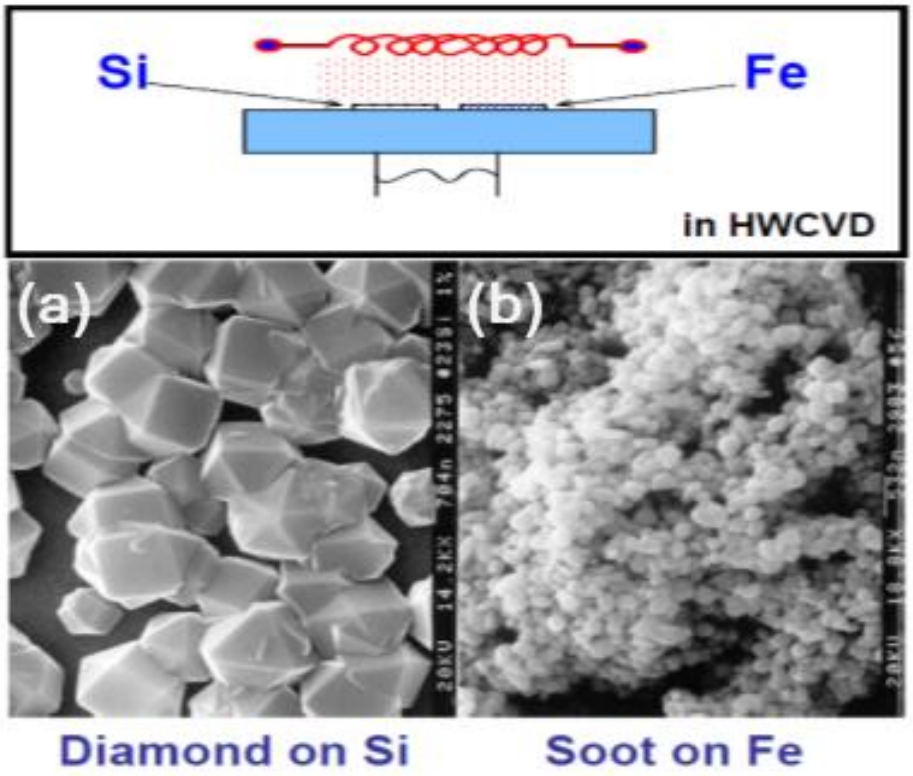

Fig. 1.1 FESEM images showing microstructures of (a) crystalline diamond deposited on the silicon substrate and (b) porous soot deposited on the iron substrate[20].

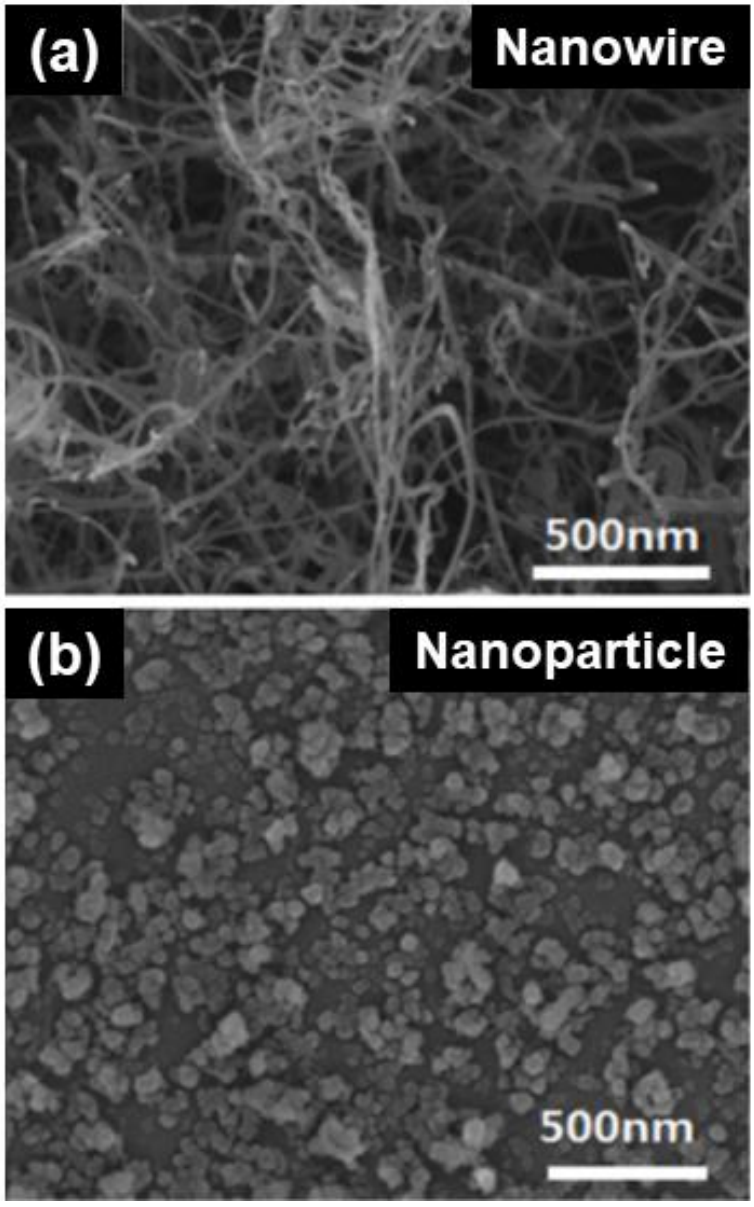

Fig. 1.2 FESEM images of (a) silicon nanowires grown on a floating silicon substrate and (b) silicon nanoparticles formed on a grounded silicon substrate[21].

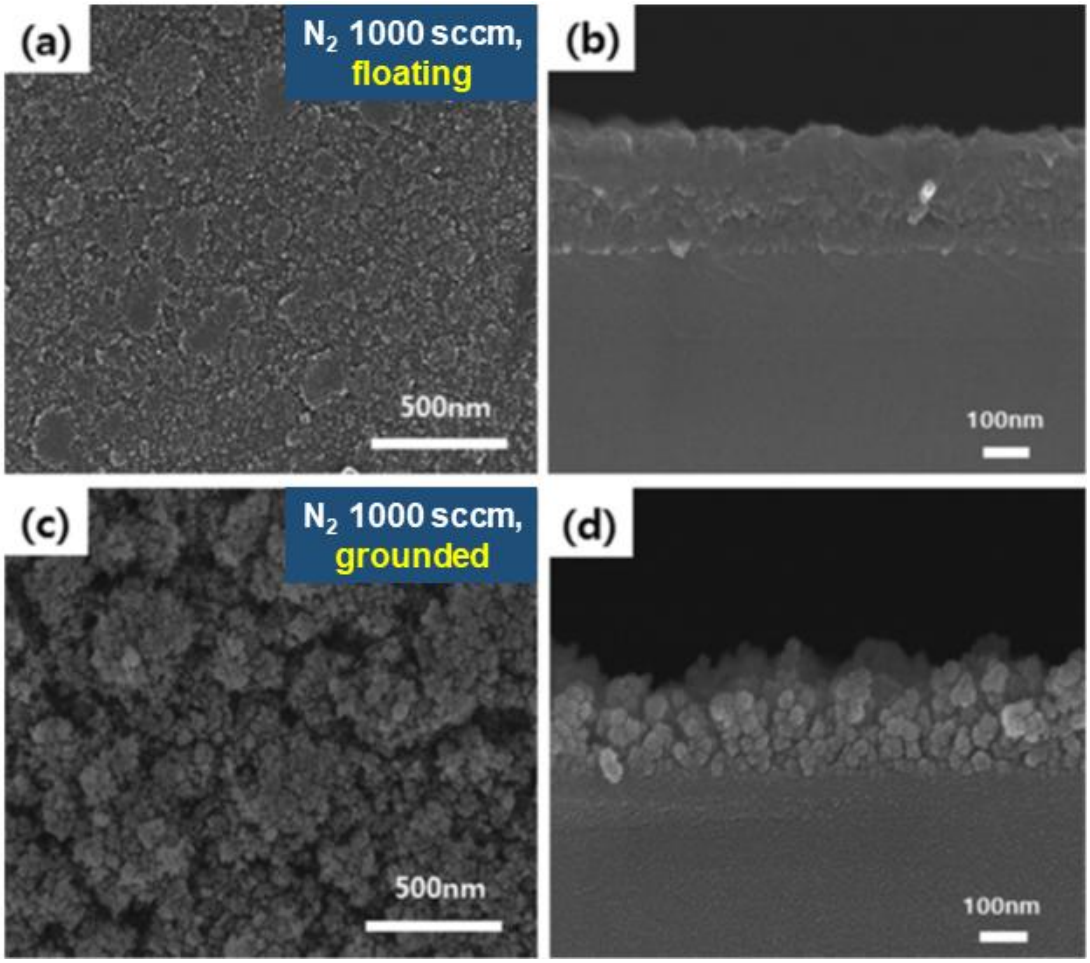

Fig. 1.3 FESEM images of (a) dense silicon film grown on a floating silicon substrate and (b) its cross section image, (c) porous silicon film grown on a grounded silicon substrate and (d) its cross section image[21].

Chapter 2.

2. Effect of bias on the low temperature growth of silicon epitaxial films during PECVD

2.1 Introduction

Silicon thin films have been extensively used in electrical devices for thin film transistor (TFTs) and thin film based solar cells[38-41]. But when they are deposited at low temperature on glass or polymer, it is difficult to obtain the polycrystalline or epitaxial silicon thin films because of the very low diffusivity of silicon atoms at low temperature[42-47]. The effect of the substrate bias was studied in the ECR-PECVD process and it was found that the positive bias improved the crystallinity or epitaxy[43, 44, 46, 47]. In these studies, however, the substrate bias was thought to attract ions or electrons; the possibility that charged nanoparticles might be generated in the gas phase and contribute to film deposition was not considered.

Until now, the deposition of films have been explained by classical crystallization based on the building block of atoms or molecules[48, 49]. However, there have been some puzzling experimental results, which cannot be properly explained by this classical crystallization[50, 51]. Rather such experimental results imply that films should be grown by the building block of nanoparticles, so called by 'non-classical crystallization'[1, 51-54]. Hwang et al.[5, 6, 13-19, 23] studied extensively the non-classical crystallization in the chemical

vapor deposition (CVD) process. In the case of the crystal growth in solution, non-classical crystallization has now become so established that its tutorial and technical sessions were included respectively in the spring meetings of Materials Research Society (MRS) and European Materials Research Society (EMRS) in 2014.

As to charging of particles, it is well established theoretically and experimentally that dust particles in the PECVD process are negatively charged[56-59]. According to measurements by Melzer et al.[57] and Trottenberg et al.[58], dust particles of 9 ~ 10 μm forming Coulomb crystals in the RF plasma contain from thousands to hundreds of thousands of elementary charge units per particle. Although micron-size particles in a plasma are known to be negatively charged, particles of a few nm are known to experience charge fluctuations[60].

As to the possibility for charging of nanoparticles, Kim et al.[61] made detailed computational analyses, which showed that most of the large particles (d = 130 nm) are charged negatively, but some fractions of small particles (d = 10 nm) are in a neutral state or charged positively. Further, based on the fact that some nanoparticles in the plasma grow so rapidly, Shiratani et al.[62] predicted that both positively and negatively charged nanoparticles should coexist. This prediction for the presence of positively charged nanoparticles was confirmed by Cabarrocas et al.[28, 63], who applied the DC bias to the substrate and showed that the deposition rate decreased as the positive bias voltage on the substrate was increased in the capacitively coupled plasma CVD (CCP-CVD) process. Cabarrocas et al.[63] found that positively charged silicon nanoparticles contributed

to 50 - 70% of deposition. This aspect was further confirmed by Yoo et al.[64], who studied the effect of the substrate bias on the deposition behavior of silicon nanoparticles in the inductively coupled plasma (ICP) CVD process.

It is known that both positively and negatively charged nanoparticles are generated in the gas phase of the PECVD process. It would be important to understand how to control the deposition of positively or negatively charged nanoparticles formed in gas phase of the PECVD process.

2.2 Experimental details

Silicon thin films were deposited using an RF-PECVD reactor as schematically shown in Fig. 2.1. The electrodes consist of upper shower head and lower substrate holder, both of which are made of stainless steel. The diameter of the disc-shaped showerhead and the side length of the square-shaped substrate holder are respectively 15 cm and 8 cm. The diameter and height of the cylindrical reactor are respectively 26.7 cm and 29.5 cm with the volume of 16.5 liter. The distance between showerhead and substrate holder is about 10 cm. The electric bias can be applied to the substrate as shown in Fig. 2.1. Substrates and membranes of TEM grids were placed on the substrate holder during the experiment.

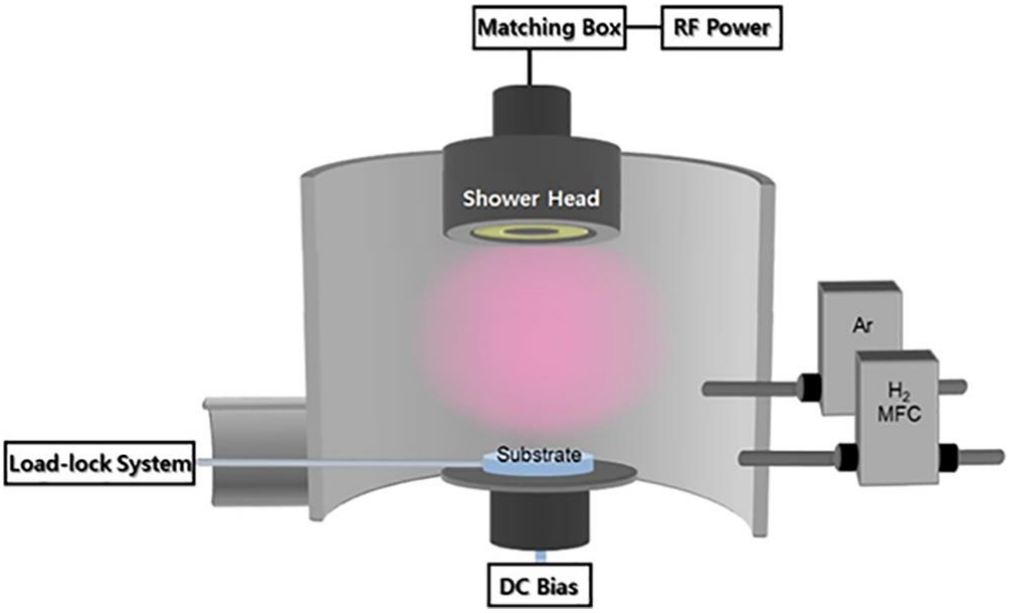

Fig. 2.1 Schematic of the PECVD reactor.

The substrate temperature was controlled with a self-regulating heating system and measured by the direct contact of a thermocouple with the substrate. The plasma power was 125 W and the reactor pressure was 1 torr. The flow rates of precursors and gases were controlled by a mass flow controller (MFC). Silane (SiH_4, 99.9999%), hydrogen (H_2, 99.9999%) and Argon (Ar, 99.999%) gases were used as precursors for deposition of silicon thin films. The flow rates of SiH_4, H_2, and Ar were respectively 2, 48 and 10 standard cubic centimeters per minute (sccm).

To examine the bias effect on the deposition behavior of silicon, silicon films were deposited on the 1 cm × 1 cm p-type (100) silicon wafers at 550 ℃ with the substrate biases of 0 V, +1000 V, and -1000 V. For epitaxial growth, the silicon wafer substrates were pretreated by dipping in a 5 % HF solution in order to remove an organic residues and a native oxide. To observe the cross sectional microstructure of the silicon films, TEM specimens were prepared using a focused ion beam (FIB, Nova 200, FEI). The cross-section of the specimens was observed by high resolution transmission electron microscope (HRTEM, F30, FEI) operated at 200 KeV.

To confirm the generation of silicon charged nanoparticles in the gas phase, they were captured for 15 sec on silicon monoxide and carbon membranes of Cu grids for TEM observation using a shutter placed above the grid membrane. The reason why silicon monoxide and carbon membranes were used was to compare the capturing behavior of charged nanoparticles between insulating and conducting substrates. The nanoparticles captured on grid membranes were observed by high resolution transmission electron microscope

(HRTEM, F30, FEI) operated at 200 KeV.

Silicon thin films were deposited on the 1 cm × 1 cm Corning Eagle XG glass, p-type (100) silicon wafer and Fe-3 wt% steel substrates with the biases of 0 V, +1000 V, and -1000 V applied to the substrate holder. In this case, the substrate temperature was chosen to be 400 ℃ so that the deposition temperature may be below the softening temperature of glass. The deposition times were 3, 5, 10, 15 minutes, respectively. The thickness of films was measured by the surface profile of Alpha-Step IQ (Rev. AL-1).

2.3 Results

Fig. 2.2 shows TEM images of the silicon film deposited on a silicon wafer by the deposition condition without bias. Fig. 2.2(a) shows an overall cross section image of the film. This image consists of two layers distinguished by the contrast. The lower grey and the upper white layers are respectively the silicon wafer and the deposited silicon film. Fig. 2.2(b) shows a magnified image of the square indicated in fig. 2.2(a). The upper whitish layer of the deposited silicon film has a columnar structure, which is partially revealed in fig. 2.2(b). This microstructure is commonly observed in silicon films deposited by CVD[65, 66]. Fig. 2.2(c) shows a HRTEM image of the interfacial region, which is the magnified image of the square indicated in fig. 2.2(b). The area of the inverted triangle indicated by the dashed line in fig. 2.2(c), which consists of a polycrystalline silicon phase, indicates the initiation of the columnar structure. Outside of the columnar structure, microcrystalline silicon,

which consists of crystalline silicon grains of a few nanometers embedded in the amorphous silicon, was deposited.

Fig. 2.3 shows TEM images of the silicon film deposited with +1000 V bias applied to the substrate holder. Fig. 2.3(a) shows an overall cross section image of the film. This image consists of three layers which are silicon wafer, epitaxial and microcrystalline layers. The dark gray triangular area was evolved from the interface between the silicon wafer and the deposited film. Fig. 2.3(b) shows the HRTEM image, which is the magnified image of the square indicated in fig. 2.3(a). The dark gray layer in the right of the dashed line in fig. 2.3(b) is a part of the triangular area of fig. 2.3(a). The gray layer in the left of the dashed line in fig. 2.3(b) is a part of the microcrystalline layer of fig. 2.3(a). Fig. 2.3(b) shows that the triangular area has a single crystal structure of same orientation with the wafer substrate, indicating that this area was grown epitaxially. Fig. 2.3(c) shows the magnified HRTEM image of the square indicated in fig. 2.3(a). Fig. 2.3(c) indicates more clearly that epitaxial growth occurred in the triangular area. However, the epitaxial growth did not continue but broke down and the microstructure changes abruptly to the microcrystalline silicon as indicated by the triangular shape shown in fig. 2.3(a) and (b).

Fig. 2.4 shows TEM images of the silicon film deposited with -1000 V bias applied to the substrate holder. Fig. 2.4(a) shows an overall cross section image of the film. This image consists of two layers. The lower and the upper layers are respectively the substrate wafer and the deposited film. Fig. 2.4(b) shows the magnified HRTEM image of the square indicated in fig. 2.4(a). Fig. 2.4(c)

shows the magnified HRTEM image of the square in the interfacial region indicated in fig. 2.4(a). Fig. 2.4(b) and (c) shows that the fully homo-epitaxial silicon film was deposited under the condition with -1000 V applied to the substrate holder. The epitaxial growth did not break down but continued to the surface of the film.

Fig. 2.3 and 2.4 indicate that epitaxial growth of silicon films is enhanced by applying the bias to the substrate although -1000 V was more favorable for epitaxial growth than +1000 V. It should be noted that a fully epitaxial film could be grown at the substrate temperature of 550 °C under the substrate bias of - 1000 V. One possibility to explain this epitaxial growth under the bias is the ionized cluster beam deposition and epitaxy (ICBE) method reported by Takagi et al.[67]. In this method, clusters are generated using the Knudsen cell and then ionized by the electron impact. The resultant ionized clusters are accelerated toward the substrate by the electric field. By ICBE, the epitaxial growth can be obtained even at low temperature.

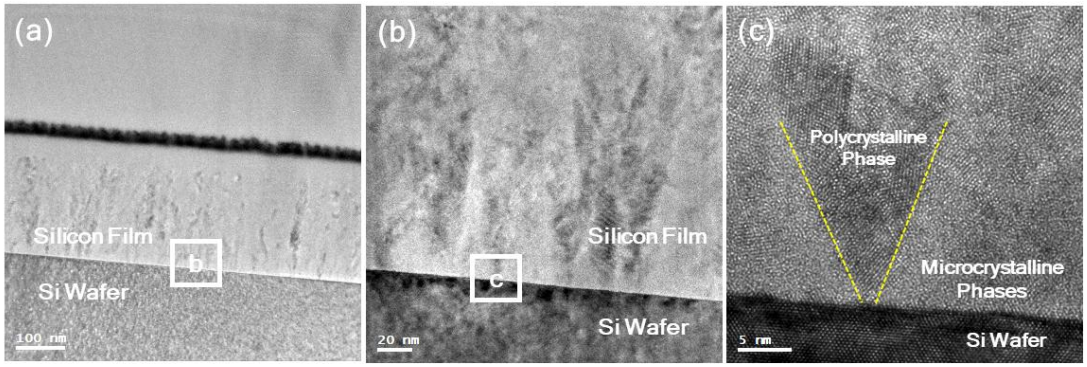

Fig. 2.2 TEM cross-section images of the silicon films on (100) silicon wafer without bias: (a) low magnification TEM image of films, (b) TEM image of the silicon of the interfacial region between silicon wafer and silicon film, and (c) HRTEM image of the interfacial region.

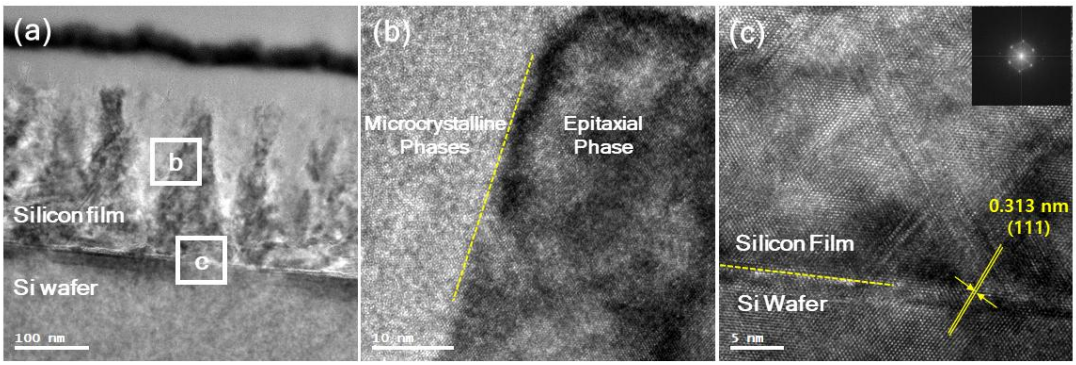

Fig. 2.3 TEM cross-section images of the silicon films on (100) silicon wafer with +1000 V: (a) low magnification TEM image of films, (b) HRTEM image of the silicon film at middle part, and (c) HRTEM image of the interfacial region.

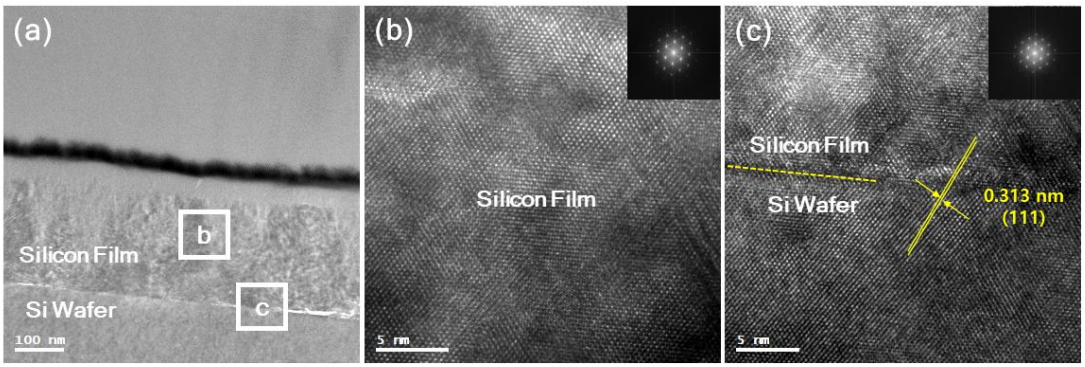

Fig. 2.4 TEM cross-section images of the silicon films on (100) silicon wafer with -1000 V: (a) low magnification TEM image of films, (b) HRTEM image of the silicon film at middle part, and (c) HRTEM image of the interfacial region between silicon wafer and silicon film.

In relation to this possibility, Hwang[68] suggested non-classical crystallization of thin films in the CVD and PVD processes, where charged nanoparticles are generated in the gas phase and become the building block of thin films. If non-classical crystallization of thin films is combined with the concept of ICBE, the partial and full epitaxial growth in figs. 2.3 and 2.4 can be explained as follows. Charged nanoparticles are generated in the gas phase of the PECVD reactor, which was experimentally confirmed by Yoo et al.[64] And these charged nanoparticles would be accelerated toward the substrate when the bias of +1000 V or -1000 V was applied to the substrate holder. Acceleration of these charged nanoparticles would favor the epitaxial growth at the relatively low substrate temperature of 550 °C.

According to this explanation, charged nanoparticles should exist in the gas phase of the RF-PECVD reactor. Their existence can be confirmed by capturing them on a membrane of the TEM grid. Fig. 2.5 shows the silicon nanoparticles captured for 15 sec on the insulating silicon monoxide membrane of the Cu grid with the bias applied to the substrate holder. Fig. 2.5(a) - (c) are the TEM images of captured nanoparticles under the biases of 0 V, +1000 V, -1000 V, relatively. The size and the amount of nanoparticles among fig. 2.5(a), (b) and (c) were not much different. However, when the bias of -1000 V was applied to the substrate holder, the nanoparticles were captured only in the center region of each membrane and the depletion zone is observed near each metal mesh as shown in fig. 2.5(c). Such a depletion zone was not observed when the biases of 0 V and +1000 V were applied. The depletion zone in fig. 2.5(c) implies that the electrostatic energy should be involved. Nanoparticles on the membrane tended to be aggregated with the size of individual

nanoparticles being in the range of 20 ~ 40 nm.

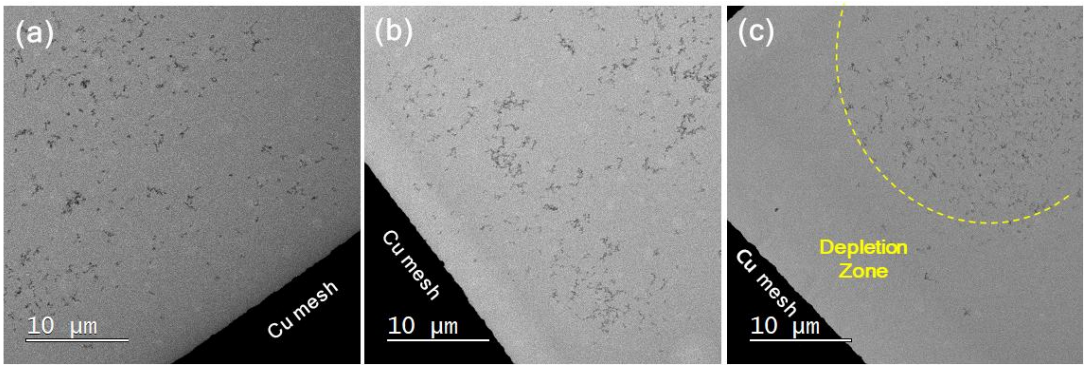

Fig. 2.5 TEM images of silicon nanoparticles captured on SiO TEM grid with an exposure time of 15 sec for (a) 0 V, (b) +1000 V, and (c) -1000 V.

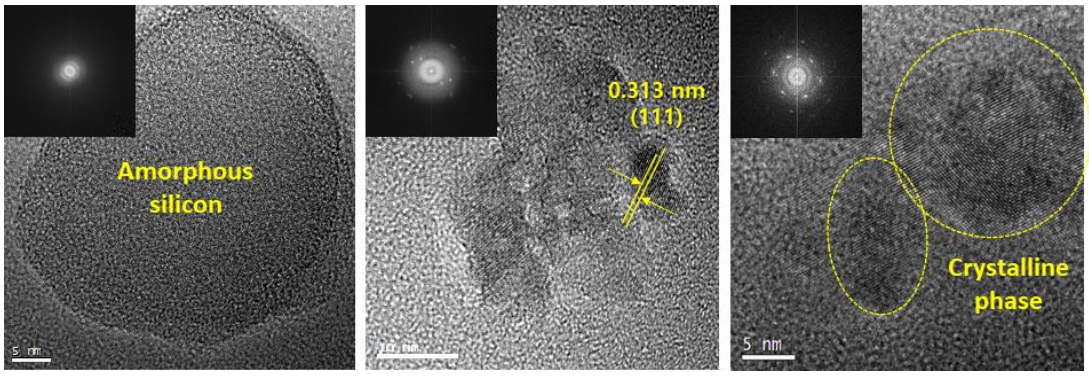

Fig. 2.6 HRTEM images of silicon nanoparticles captured on SiO TEM grid with an exposure time of 15 sec for (a) 0 V, (b) +1000 V, and (c) -1000 V.

Fig. 2.6 shows that the HRTEM images of silicon nanoparticles shown in fig. 2.5. The HRTEM image of fig. 2.6(a) shows that nanoparticles captured without the substrate bias are mostly amorphous. The HRTEM image of fig. 2.6(b) shows that nanoparticles captured under the bias of +1000 V had a higher fraction of crystalline silicon than that of amorphous silicon. Also in fig. 2.6(c) where the bias of －1000 V was applied, nanoparticles had a higher fraction of crystalline silicon.

Figs. 2.7(a), (b) and (c) show the silicon nanoparticles captured for 15 sec on the conducting carbon membrane of the Cu grid with substrate biases of 0 V, +1000 V, and －1000 V, respectively. It should be noted that nanoparticles were captured on the membranes of figs. 2.5 and 2.7 simultaneously in the PECVD reactor. Therefore, except the conductivity of the membrane, the capturing condition of the carbon membrane of fig. 2.7 was the same as that of fig. 2.5. However, the capturing behavior on the conducting carbon membrane in Fig. 2.7 was quite different from that on the insulating silicon monoxide membrane in Fig. 2.5. As in figs. 2.5(a), (b) and (c), the size and the amount of nanoparticles were not much different among figs. 2.7(a), (b) and (c). However, the amount of nanoparticles was much larger than that of fig. 2.5. Besides, the depletion zone was not observed. Such differences between figs. 2.5 and 2.7 would come from the difference in the conductivity of the membranes.

Figs. 2.8(a), (b) and (c) are respectively the HRTEM images of silicon nanoparticles in figs. 2.7(a), (b) and (c). In fig. 2.8(a), where nanoparticles were captured without the bias, nanoparticles are mostly amorphous. In figs. 2.8(b) and (c), where nanoparticles were captured

respectively under the biases of +1000 V and -1000 V, nanoparticles have a higher crystalline fraction than an amorphous fraction.

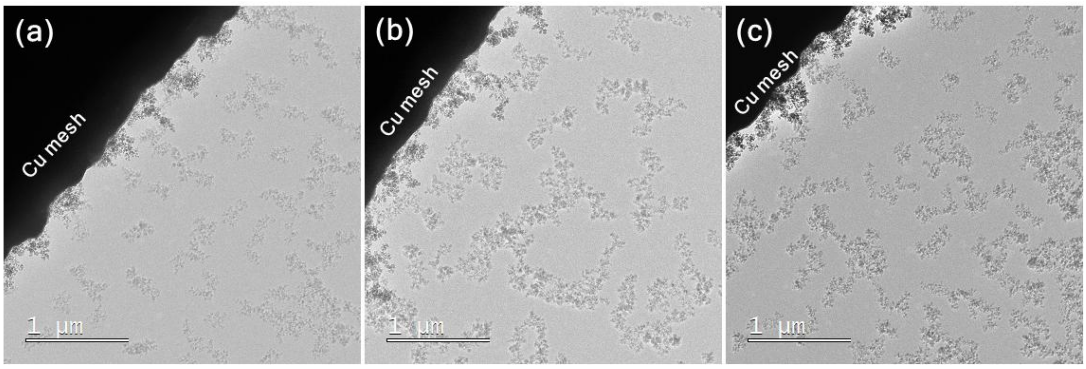

Fig. 2.7 TEM images of silicon nanoparticles captured on carbon TEM grid with an exposure time of 15 sec for (a) 0 V, (b) +1000 V, and (c) -1000 V.

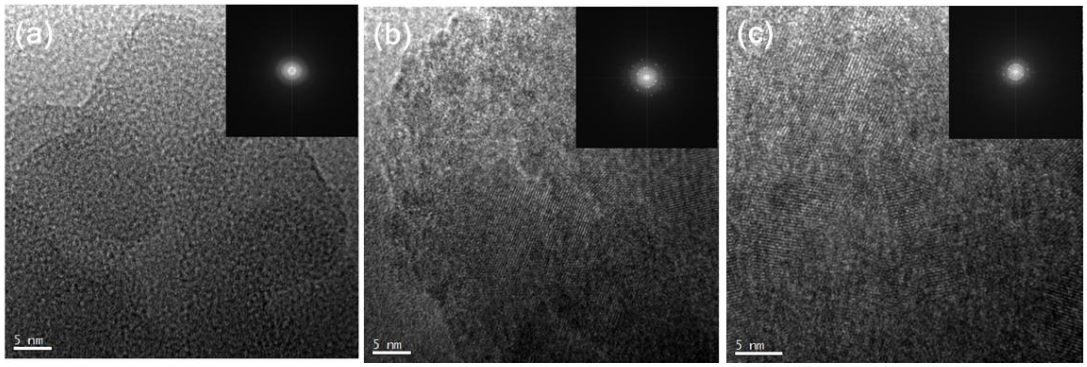

Fig. 2.8 HRTEM images of silicon nanoparticles captured on carbon TEM grid with an exposure time of 15 sec for (a) 0 V, (b) +1000 V, and (c) -1000 V.

Since the capturing behavior depended on the bias and the conductivity of the membrane substrate, three substrates of glass, silicon wafer and Fe alloy, which are respectively insulating, semiconducting and conducting, were used to compare the deposition rate. After the deposition for 15 min, the deposition rates on glass, silicon wafer and Fe alloy at 400 ℃ were respectively 1.50, 1.74 and 2.64 under the deposition condition without the bias as shown in fig. 2.9. Under the deposition condition of the biases of +1000 V and -1000 V, the deposition rate was increased remarkably from 2.64 Å/s respectively to 3.93 and 3.99 Å/s on the conducting Fe alloy substrate. However, the deposition rate was increased only marginally from 1.50 Å/s to 1.70 Å/s for +1000 V and 1.74 Å/s for -1000 V on the insulating glass substrate and from 1.74 Å/s to 1.89 Å/s for +1000 V and 1.93 Å/s for -1000 V on the semiconducting silicon wafer substrate as shown in fig. 2.9. Fig. 2.9 also shows that the conducting Fe alloy has a much higher deposition rate than the insulating glass and the semiconducting silicon wafer, which is consistent with the results of figs. 2.5 and 2.7, where the amount of captured nanoparticles is much higher on the conducting carbon membrane than on the insulating silicon monoxide membrane.

In fig. 2.9, the bias effect on the deposition rate is appreciable on the conducting Fe alloy whereas it is only marginal on the insulating glass and the semiconducting silicon wafer. In order to examine the effect of the conductivity of the substrate material on the deposition rate under the bias condition in more detail, the deposition rate was measured using the surface profile of Alpha-Step IQ with the deposition times of 3, 5, 10 and 15 min.

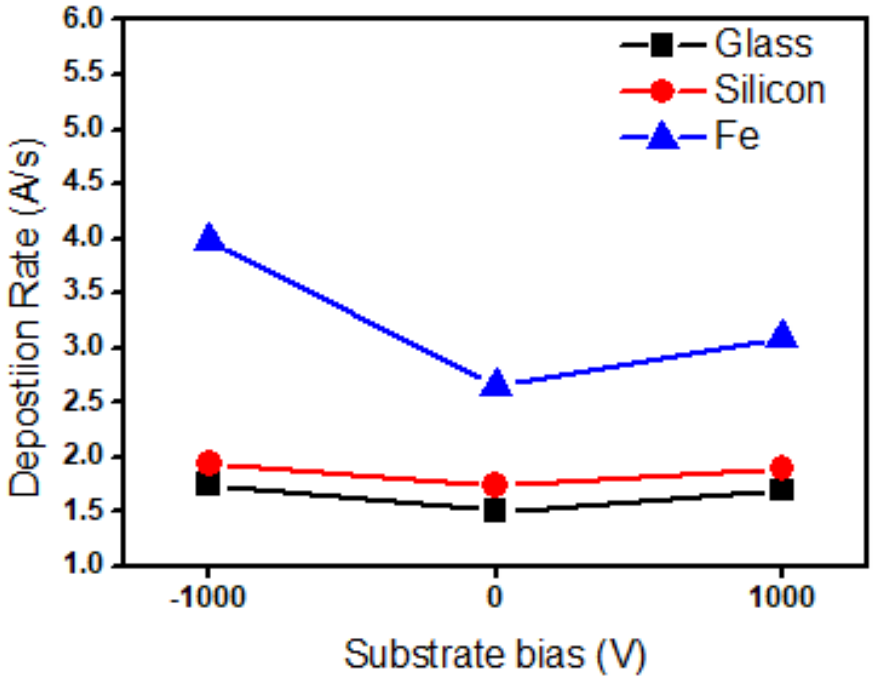

Fig. 2.9 The growth rate of silicon films prepared with various substrates at 400 °C and bias for 15 min.

Fig. 2.10(a), (b) and (c) show the variation of the deposition rate with the deposition time respectively on glass, silicon wafer and Fe alloy under the substrate biases of 0 V, +1000 V, and －1000 V. Fig. 2.10(a) shows that the deposition rate without the bias does not vary much with the deposition time. Under the biases of +1000 V and －1000 V, however, the deposition rate is high in the early stage of deposition but decreases with time. It should be noted that fig. 2.10 shows the average deposition rate, which is determined by the thickness divided by the deposition time. If the instantaneous deposition rate, which is determined by the slope in fig. 2.10 or by the incremental thickness divided by the incremental time, is considered, the deposition rate at 15 min with the bias would be practically the same as that without the bias although the average deposition rate at 15 min with the bias is a little bit higher than that without the bias in fig. 2.10. In other words, the deposition rate would not change much after 15 min regardless of the bias although the films deposited under the bias are thicker than those without the bias.

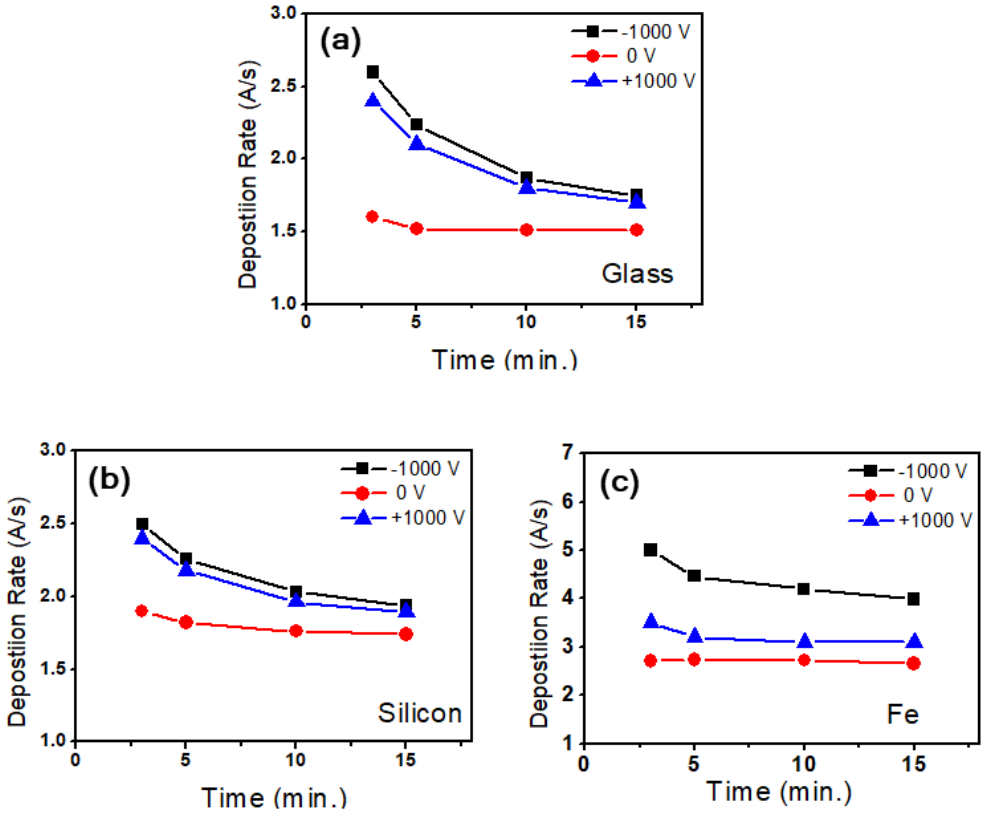

Fig. 2.10 (a) The growth rate of silicon films on the glass substrate at various time, (b) The growth rate of silicon films on the silicon wafer at various time, (c) The growth rate of silicon films on the Fe substrate at various time.

2.4 Discussion

The amount of captured nanoparticles on the conducting carbon membrane in fig. 2.7 is much larger than that on the insulating SiO membrane in fig. 2.5 indicates that these nanoparticles are charged. Nanoparticles on the SiO membrane in fig. 2.5 and those on the carbon membrane in fig. 2.7 are amorphous when the bias was not applied but crystalline when the bias was applied. This result is important in relation to understanding the formation mechanism of crystalline silicon at low temperature in the RF-PECVD process. One possible explanation for crystalline nanoparticles captured on the membrane under the bias would be the acceleration of charged nanoparticles by the applied bias. Consider two cases where nanoparticles in the gas phase are amorphous and crystalline. Before discussing further, it should be reminded that the acceleration of nanoparticles toward the substrate tends to favor their transformation to the substrate structure, which is the underlying principle of ICBE.

In the case where charged nanoparticles in the gas phase are amorphous, the acceleration of them toward the amorphous membrane would not favor their transformation to crystalline silicon. In the case where charged nanoparticles in the gas phase are crystalline, the crystallinity can be lost or maintained even after their acceleration toward the amorphous membrane. Crystalline nanoparticles captured on amorphous membranes under the bias in figs. 2.5(b) and 2.5(c) and in figs. 2.7(b) and 2.7(c) indicate that nanoparticles in the gas phase must have been crystalline. However, nanoparticles captured on amorphous membranes without the bias in figs. 2.5(a) and 2.7(a) are not crystalline but amorphous at least in our observation by TEM.

This result implies that nanoparticles in this case should be amorphous in the gas phase.

Therefore, some nanoparticles are crystalline and other nanoparticles are amorphous in the gas phase. And amorphous nanoparticles are captured on the membrane in the absence of the bias and crystalline nanoparticles are captured under the bias. How would nanoparticles differ between the presence and absence of the bias? In the presence of the bias, nanoparticles with a large amount of charge would be attracted toward the membrane whereas in the absence of the bias, nanoparticles with a small amount or absence of charge would land on the membrane. This means that nanoparticles with a large amount of charge would be crystalline whereas nanoparticles with a small amount or absence of charge would be amorphous. In other words, charge induces crystallization of nanoparticles and this effect is enhanced when the amount of charge per nanoparticle is increased. This possibility of charge-induced crystallization of nanoparticles is in agreement with the previous TEM observation of gold nanoparticles showing that charged nanoparticles tended to make liquid-like coalescence[69], whose aspect was attributed to weakening the bond strength by charge[68, 72]. It should be noted that such a role of charge in making nanoparticles liquid-like is critical to the non-classical crystallization by the building block of charged nanoparticles[68].

On the other hand, epitaxial growth of silicon is most favored under the bias of －1000 V as shown in figs. 2.2 – 2.4 and the fraction of crystalline nanoparticles captured on the SiO and carbon membranes is highest also under the bias of －1000 V as shown in

figs. 2.5 – 2.8. However, the size of captured nanoparticles was more or less the same. This implies that positively charged nanoparticles are more favorable in producing an epitaxial film than negatively charged nanoparticles, which indicates that the former has stronger tendency of liquid-like coalescence than the latter. One possible explanation would be that the amount of charge on the positively-charged nanoparticles should be larger than that on the negatively-charged nanoparticles. As a result, a larger amount of charge would make positively-charged nanoparticles more liquid-like and more crystalline, providing the favorable condition for epitaxial film growth.

There is another factor to be considered. It is known that in the RF-PECVD system, the DC negative bias is naturally applied to the small substrate electrode because electrons have a much higher mobility than ions. As a result, the chamber wall including the substrate would be negatively charged, which produces a floating potential. Again, the floating potential produces 'self bias'[71, 72]. It should be noted that in our experiment, the upper shower head electrode is roughly 3 times larger than the lower substrate electrode. Therefore, it is expected that the self bias would be imposed on the lower electrode. This self bias would be added to the DC bias applied to the substrate on the small electrode. The negative self bias was measured by the RF matching network controller and the values were 68 V under the bias of – 1000 V, 57 V under the bias of 0 V and 23 V under the bias of +1000 V. Therefore, the electric field under the condition of negative bias is higher than that of positive bias. The positive and negative DC biases applied to the substrate would be respectively decreased and increased by the self bias. Under the

condition where both positively and negatively-charged nanoparticles carry the same amount of charge, the negatively-biased substrate holder would attract positively-charged nanoparticles more strongly toward the growing surface of the silicon film and simultaneously the positively-biased substrate holder would attract negatively-charged nanoparticles less strongly. Again, this factor would favor the epitaxial growth of silicon films on the negatively-biased substrate in fig. 2.4.

The depletion zone on the insulating SiO membrane in fig. 2.5(c), which is absent on the conducting carbon membrane in fig. 2.7(c), can also be approached by the hypothesis that nanoparticles are multiply charged. It appears that the flux of positively-charged nanoparticles is attracted toward the conducting Cu mesh and, as a result, becomes depleted in the area of the SiO membrane near the Cu mesh. This would be attributed to the fact that under the condition of the bias applied to the conducting holder, the conducting Cu mesh produces a higher electric field than the insulating SiO membrane. Then, why isn't there the depletion zone in the case of positive bias in fig. 2.5(b)? As mentioned before, the amount of charge on negatively-charged nanoparticles is smaller than that on positively-charged nanoparticles and the electric field produced by the negative bias is higher than that by the positive bias due to the self bias formed in the RF-PECVD process.

Fig. 2.9 shows that the Fe substrate has a higher deposition rate than glass and Si substrates. The reason might be that the Fe substrate has a high conductivity so that the charge buildup on the substrate would be minimized. This result implies that the charge

removal might be the rate-determining step in the deposition of Si films in PECVD. A little bit higher growth rate on Si than on glass in fig. 2.9 would also be attributed to the fact that the charge buildup on the Si substrate would be less than that on the glass substrate. On the other hand, fig. 2.9 shows that the effect of the applied bias on the film growth rate is more pronounced on the Fe substrate than on the Si and glass substrates. This might be due to the fact that the bias effect would be diminished on the insulating substrate, where charge tends to buildup. For example, when +1000 V is applied to the holder of the glass substrate, the negative charges would land on the glass substrate. Because of this negative charges, most of the electric field made by the bias of +1000 V would be cancelled.

The decreased deposition rate on glass with time in fig. 2.10(a) would be related with the charge buildup on the insulating substrate. When +1000 V is applied to the substrate holder, negatively charged electrons, ions and nanoparticles would be attracted to the glass substrate and the positively charged species would be repelled from the substrate. The negative charges built up on the glass surface would diminish the electric field produced by the applied bias. As a result, the bias effect would be diminished with the deposition time. Then, the instantaneous deposition rate with the bias would approach the rate without the bias at 15 min of deposition as shown in fig. 2.10(a). In other words, the steady state of charge buildup is reached at 15 min of deposition.

The decreased effect of the bias on the deposition rate with time is also observed for the silicon wafer and Fe substrates as shown respectively in figs. 2.10(b) and (c). However, this tendency decreases

for the silicon wafer and even further for the Fe. Considering the conductivity of the Fe, the charge buildup would not occur on the surface. However, when the silicon film deposits on the Fe substrate, the charge buildup would occur on the growing silicon surface. This would be why the deposition rate under the bias condition decreases slightly with time in fig. 2.10(c).

2.5 Conclusion

Fully homo-epitaxial silicon films could be deposited at 550 ℃ by applying the bias of -1000 V to the substrate holder. The deposition behavior depended on the substrate bias and the conductivity of the substrates. The negative substrate bias seems to attract charged nanoparticles most strongly because the amount of charge of positively-charged nanoparticles is higher than that of negatively-charged nanoparticles and at the same time the negative bias produces a higher electric field because of the self bias in the RF-PECVD. These conditions seem to favor the growth of silicon epitaxial films.

Chapter 3.

3. Comparison of plasma effect on dewetting kinetics of metal films between floating and grounded states

3.1 Introduction

Solid metal thin films in the as-deposited state are in the very high energy or unstable state. When sufficient external energy such as thermal heating, laser source or plasma treatment is given, they tend to decrease their interfacial free energy by dewetting or agglomeration on the substrate[73]. Traditionally, solid-state dewetting using thermal heating as an energy source has been widely studied[74-76]. To understand how solid-state dewetting initiates and proceeds, a mechanism of hole nucleation and growth has been suggested. Hole nucleation takes place where the energy of film is high, especially at the location such as triple junction lines, where three grains meet in the polycrystalline structure. It happens when the film temperature is in the solid state or below the melting temperature. But recently, Kwon et al.[77] and Choe et al.[78] found out that the plasma treatment markedly enhances the dewetting rate. Compared with thermal heating, the plasma treatment not only enabled the film to undergo a much faster dewetting process but also produced a highly uniform dewetting structure. They attributed the enhanced dewetting kinetics to ion or electron bombardments on the surface.

On the other hand, it has been found out that many thin films and

nanostructures grow by charged nanoparticles formed in the gas phase[21, 23, 31, 55]. In other words, charged nanoparticles can be the building block in the growth of films or nanowires. Such crystal growth by the building block of nanoparticles has been observed in many systems not only in the gas phase but also in solution and called 'non-classical crystallization'[10,68]. In non-classical crystallization, one of the important issues is that how dense films without any voids or nanowires with smooth surface can grow by the building block of nanoparticles. One possibility suggested by Hwang[68] is that charged nanoparticles should have a liquid-like property and the presence of charge in nanoparticles should enhance the diffusion kinetics.

In relation to this possibility, Iijima made in-situ transmission electron microscopy (TEM) observation that gold nanoparticles containing 459 atoms under electron irradiations by TEM showed the liquid-like behavior, constantly transforming themselves into such as face centered cubic, tetragonal, cuboctahedral, multiply twinned icosahedral structures[69]. However, the dynamic motion of the particles became sluggish when an electrically good conductor such as graphite or amorphous carbon was used as a substrate[79]. Alumina substrates gave the same results as the SiO_2-covered Si but almost no activities of the clusters were observed when a conducting substrate was used. Considering the fact that the evolution rate of particles depends on the conductivity of the substrate, the active movement comes from the amount of charge buildup rather than from the electron bombardment. Iijima and Ichihashi proposed that the state of such a small particle should be called 'quasi solid state', which is neither solid nor liquid according to the conventional concepts of

matter[69]. Since these results indicate that the charged nanoparticles should have a liquid-like property, Kim made a detailed study by comparing the dynamic behavior of the Au nanoparticles between conducting and insulating substrates by in-situ TEM[80]. The study showed that electric charges are responsible for the liquid-like behavior of Au nanoparticles.

Considering these results, there is a possibility that the dewetting kinetics enhanced by plasma treatment might not come from ion or electron bombardments but come from the charge buildup on the film surface. The purpose of this paper is to clarify whether the enhanced kinetics by plasma should come from ion bombardments or charge buildup. For this, the dewetting behavior of Au and Sn films on the silicon substrate with a native oxide surface was compared between electrically floating and grounded states by exposing Au and Sn films to inductively-coupled plasma. Then, Sn film on elongated silicon substrate attached with Al conducting tape was exposed to inductively-coupled plasma. Also, the DC bias was applied to the stainless substrate holder to see the effect of the charge buildup by the electric bias on the diffusion kinetics of a Sn film.

3.2 Experimental details

Au films and Sn films were deposited on 1 cm × 1 cm p-type (100) silicon wafers by conventional DC magnetron sputtering with 99.9999 % pure targets. For Au films, the deposition time was 20 sec with the DC power of 20 W, which produces the film thickness of 3 nm. For Sn films, the deposition time was respectively 120 and 240

sec with the DC power of 20 W, which produces the film thickness of 100 and 200 nm.

To compare the effect of plasma on the dewetting kinetics between floating and grounded films, the two samples were placed on the stainless substrate holder which is in contact with the grounded stainless chamber. One sample with an Au film was made grounded by attaching a conducting Al tape over the edge of the film as shown schematically in fig. 3.1(a) whereas the other sample was made floating caused by the insulating native oxide on the silicon substrate as shown in fig. 3.1(b). For the grounded film, ~ 1 mm width of the film edge was covered by the Al tape. The glue of the tape was made of acrylic adhesives and it was conducting. After the experiment, the tape was separated from the film, and the glue still remained on the tape. We analyzed the composition of the film by EDS but we could not find any impurities suspected to come from the glue of the tape.

When the two samples were exposed to plasma, energetic ions and electrons would bombard the film surface and the plasma heating would increase the temperature. In order to check any temperature difference between grounded and floating films, a K-type thermocouple was used. Since the tip of the thermocouple should not be in contact with the Sn film to prevent it from going short, it was placed at 1 mm above both films. When the plasma was turned on for 1 min, the temperatures 1 mm above both films were measured to be 57 °C, not showing any difference. After 2 min, the temperatures were increased to 84 °C but did not show any difference between floating and grounded films. To check the

temperature gradient in the vertical direction, the temperatures at 11 mm above the films were also measured, which was 61 °C and 91 °C respectively after the plasma was turned on for 1 min and 2 min. Therefore, it is expected that the film temperature was less than 60 °C for 1 min of dewetting experiments.

In addition to the bombardment effect of energetic ions and electrons, there would be an effect of charge buildup. The charges would not tend to build up on the surface of the grounded film because charges from the plasma will easily migrate through the tape to the stainless substrate holder (fig. 3.1(a)) whereas the charge would tend to build up on the surface of the floating film (fig. 3.1(b)). Then, the two substrates were exposed to plasma simultaneously with inductively coupled plasma (ICP) source for 60 sec. The RF plasma power was 500 W and the operating pressure of the reactor was 30 mtorr. The flow rate of gas was controlled by a mass flow controller (MFC). Hydrogen (H_2, 99.9999%) was supplied at 30 standard cubic centimeters per minute (sccm). The role of hydrogen was not only to generate the plasma but also to prevent the oxidation of Sn, since solid state dewetting of metal thin films is strongly inhibited by oxidation[81]. And the potential of the floating film was measured to be 7 V. In order to check the reproducibility of dewetting experiments, the dewetting kinetics was compared between floating and grounded Sn films. To investigate further the influence of charge on the dewetting kinetics, Sn films were deposited by sputtering on two elongated silicon substrates of 1 cm x 3 cm with one end grounded by the conducting Al tape to the stainless substrate holder as shown schematically in fig. 3.6(a). Then, the specimen was exposed to the plasma of 500 W for 2 min.

As another means to build up charge on the Sn film, the DC bias of −8500 V was applied to the stainless steel substrate holder on which the silicon substrate deposited by a Sn film is attached. Because the insulating native oxide layer on the silicon substrate can prevent the bias from being properly applied to the Sn film, the substrate was placed upside down so that the Sn film can face the substrate holder as shown schematically in fig. 3.7(a). Under this condition, the sample was heated at 300 °C, for which it took 15 min. The sample was held at 300 °C for 2 h in a tube furnace at atmospheric pressure under 500 sccm of flowing H_2. For comparison, the sample without the bias was also heated under the same condition. In order to check the possibility of superheating of the Sn film, a pure Sn granule was put together with the sample into the chamber. The morphology of the films was characterized by field emission scanning electron microscope (FESEM) (ZEISS, SUPRA).

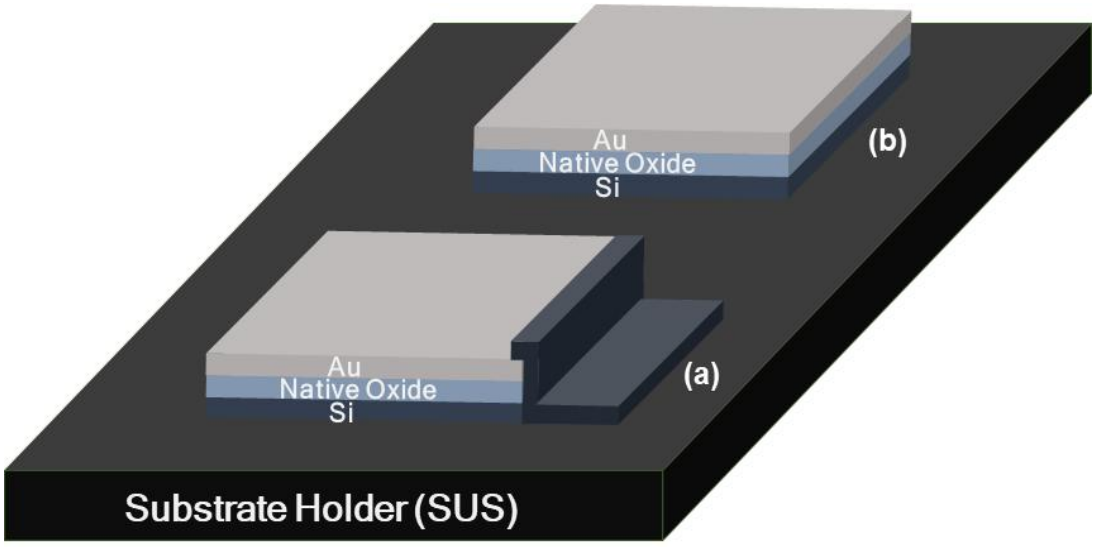

Fig. 3.1 A schematic of the experiment to compare the effect of plasma on the dewetting kinetics between (a) grounded and (b) floating Au films. In (a), the Au film is grounded by a conducting Al tape.

3.3 Results

Fig. 3.2 is the FESEM image showing how the surface morphology of the grounded Au thin films is evolved with H_2 plasma treatment. Au particles in fig. 3.2(a) are completely isolated each other although some of them have an oval shape or slightly non-spherical, indicating that the dewetting is not yet completed. In contrast, none of Au particles in fig. 3.2(b) are isolated and no islands exist, indicating that the dewetting is far from the final stage. Again, the dewetting kinetics of the floating Au film (fig. 3.2(a)) is much faster than that of the grounded Au film (fig. 3.2(b)).

There would be no difference in the amount of bombardments by the high energy species such as electrons, ions or neutrals generated in the plasma between floating and grounded surfaces. Since electrons have a much higher mobility than ions, electrons are known to occupy all the surface inside the plasma chamber. The concentration of electrons would be much higher on the floating surface than that on the grounded surface. Electrons occupying on the surface would repel the incoming electrons of high energy by Coulomb repulsion. This repelling force would be much stronger on the floating surface than on the grounded surface. The bombardment effect by the high energy electrons would be much weaker on the floating surface than on the grounded surface. Therefore, fig. 3.2, where the dewetting kinetics is much more enhanced on the floating film than on the grounded film, cannot be explained by the bombardment of the high energy electrons.

Fig. 3.3 is the FESEM image showing how the surface morphology

of the grounded Sn thin films is evolved with H_2 plasma treatment. Fig. 3.3(a) shows the surface of the as-deposited film, which consists of sub-micron size grains. Fig. 3.3(b) shows the surface of the film exposed to plasma for 30 sec. The film begins to split and the holes are generated. Fig. 3.3(c) shows the surface of the film exposed to plasma for 60 sec. Comparing fig. 3.3(c) with fig. 3.3(b), there is no appreciable change in the surface morphology.

Fig. 3.4 shows the FESEM image of the surface morphology of the Sn thin films evolved on a floating substrate with H_2 plasma treatment. The morphological evolutions of fig. 3.4 are drastically different from those of fig. 3.3. Fig. 3.4(a) shows the surface of the as-deposited film. Fig. 3.4(b) shows the surface of the film exposed to plasma for 30 sec. In fig. 3.4(b), the film is divided into many islands. Fig. 3.4(c) shows the surface of the film exposed to plasma for 60 sec. Comparing fig. 3.4(c) with fig. 3.4(b), island grains change from irregular to spherical shapes. Dewetting of the film in fig. 3.4(c) is mostly completed, producing spherical shape particles. The drastically high dewetting rate in fig. 3.4 in comparison with fig. 3.3 would come from the charge buildup on a floating substrate in fig. 3.4. This result indicates a possibility that the charge buildup should enhance the dewetting kinetics.

The drastic difference in dewetting kinetics between grounded and floating Sn films was reproduced for the different film thickness. For example, fig. 3.5 shows FESEM image of the surface morphology comparing the dewetting kinetics between floating and grounded Sn films of 200 nm thickness for the plasma power of 500 W. Similar to the results of figs. 3.3 and 3.4, the dewetting kinetics on the floating

Sn film is much faster than that on the grounded one. If fig. 3.4(c) is compared with fig. 3.5(a), it can be said that it took a much longer time for detwetting of 200 nm thick Sn film at the plasma power of 500 W to complete than for dewetting of 100 nm thick film at 500 W.

To study the effect of charge buildup further, the elongated silicon substrate of 1 cm × 3 cm was used and one end of the substrate was grounded by making the conducting path using the Al tape between the Sn film and the stainless holder as shown schematically in fig. 3.6(a). The sputter-deposited Sn film on the substrate was exposed to H_2 plasma for 2 min.

Figs. 3.6(b), (c) and (d) are the FESEM images showing how the surface morphology changes with distance from the Al tape. Figs. 3.6(b), (c) and (d) show the surface morphology of the film respectively closest to the Al tape, at the middle and farthest from the Al tape. Dewetting kinetics of the Sn thin film is slowest in fig. 3.6(b), which represents the area closest to the Al tape. Small particles in fig. 3.6(b) are Sn particles in the early stage of dewetting, in which Sn thin film breaks into many islands, changing or coalescing into spherical particles. This happens not only in the grounded film but also in the floating film. However, in fig 3.6(c) which represents the area at the middle, the Sn film was disintegrated and coalesced appreciably and the island Sn particles have an irregular shape. In fig. 3.6(d) which represents the area farthest from the Al tape, most Sn particles have an oval shape, indicating the final stage of dewetting. The charge buildup would be minimum at the area of fig. 3.6(b) and maximum at the area of fig.

3.6(d). Therefore, the result of fig. 3.6 also indicates a possibility that the charge buildup should enhance the dewetting kinetics.

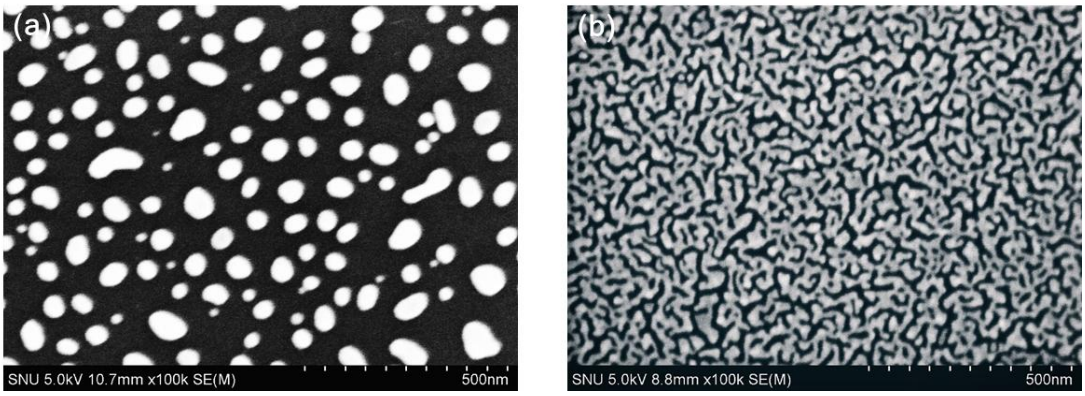

Fig. 3.2 FESEM image showing the dewetting behavior of (a) floating and (b) grounded Au films of 3 nm thickness after being exposed to plasma for 60 sec.

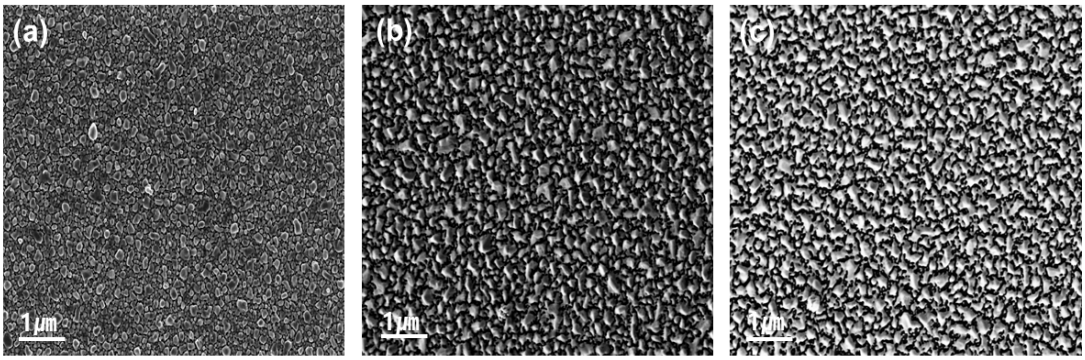

Fig. 3.3 FESEM images of the Sn films grounded by an Al tape after H_2 plasma treatment. (a) as-deposited film, (b) plasma treated for 30 sec, and (c) plasma treated for 60 sec.

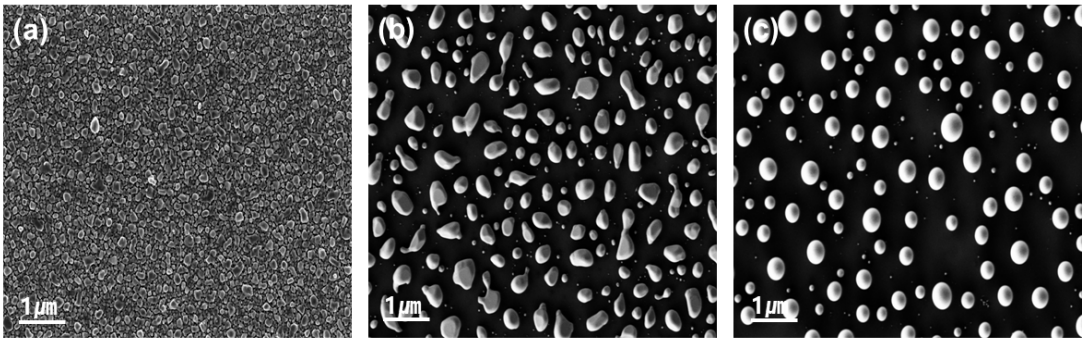

Fig. 3.4 FESEM images of the electrically floating Sn films after H_2 plasma treatment. (a) as-deposited film, (b) plasma treated for 30 sec, and (c) plasma treated for 60 sec.

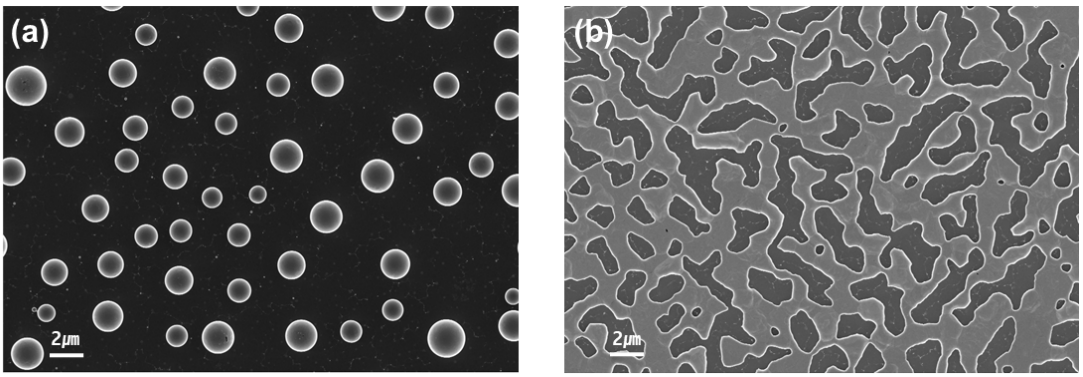

Fig. 3.5 FESEM images of the 200 nm thick Sn films after 500W power of H_2 plasma treatment for 2 min. (a) floating film, (b) grounded film.

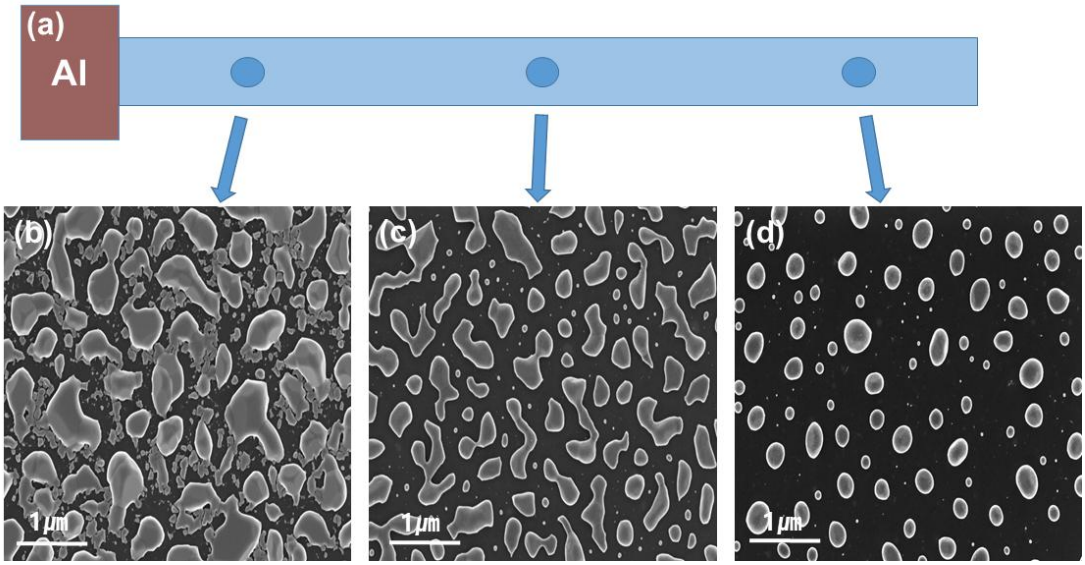

Fig. 3.6 (a) A schematic of the experiment using the elongated silicon substrate. Above are FESEM images of the elongated Sn film grounded by an Al tape after H_2 plasma treatment for 2 min. (b) the area closest to the conducting Al tape, (c) the area at the middle, and (d) the area farthest from the conducting Al tape.

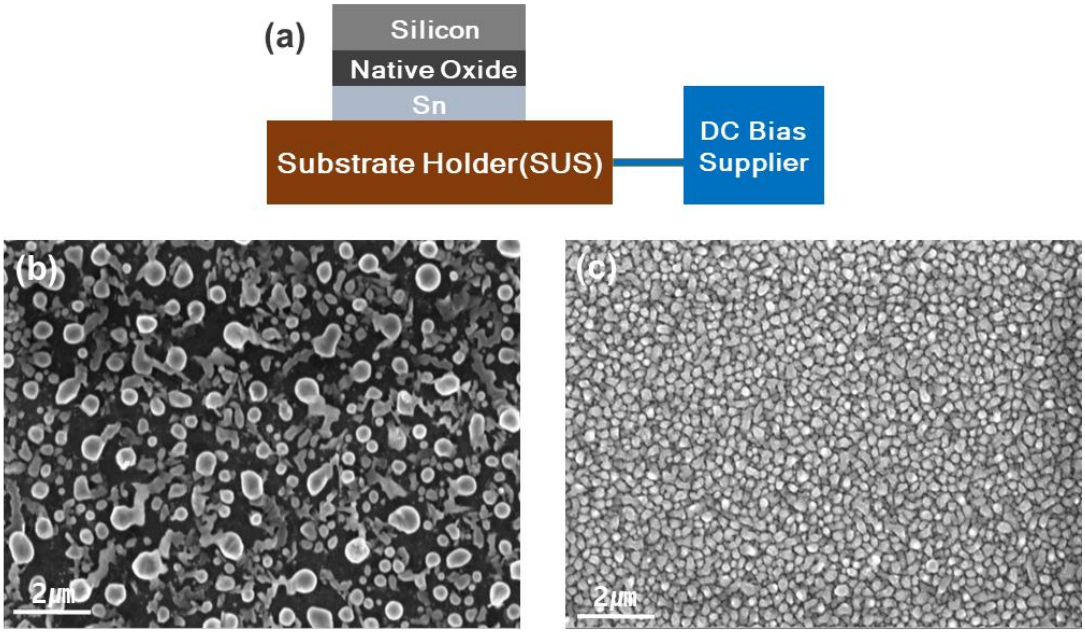

Fig. 3.7 (a) A schematic of the experiment to induce the charge building up by applying DC bias to the sample, which is heated 300 ℃ and held for 2 h. Above are FESEM images of (b) the sample applied by -8500 V and (c) the sample without bias.

Figs. 3.2 - 3.6 indicate that the charge buildup by plasma enhances the dewetting kinetics. Then, a question arises as to whether the dewetting kinetics can also be enhanced by another means of the charge buildup. The charge buildup can also be made by electric bias. To check whether the charge buildup made by electric bias might also enhance the dewetting kinetics of a Sn film, -8500 V was applied to the stainless substrate holder, which faces the Sn film as shown schematically in fig. 3.7(a). At the same time, the sample was heated to 300 ℃ and held for 2 h under which condition an appreciable change of the microstructure was observed as shown in fig. 3.7(b). For comparison, the sample without the bias was also heated under the same condition. As shown in fig. 3.7(c), the film microstructure changed much less than that of fig. 3.7(b). Comparing fig. 3.7 with figs. 3.2 - 3.6, the effect of the charge buildup by the electric bias on dewetting kinetics is not so pronounced as that by plasma. Nonetheless, fig. 3.7 provides another evidence that the charge buildup should enhance dewetting kinetics of a Sn film.

3.4 Discussion

It had been reported that solid-state dewetting kinetics of metal thin films by plasma is enhanced due to ion bombardment[77, 78, 82]. Ion bombardment would also play a role in enhacing the dewetting kinetics. This effect would be revealed if the dewetting kinetics of the grounded film is compared with that of the film which is heated to the same temperature but not exposed to plasma. Definitely, the dewetting kinetics of the film without plasma would be extremely

slower than that of the grounded film. When the film is exposed to plasma, however, both effects of ion bombardment and charge on dewetting kinetics are mixed. Both surfaces of floating and grounded films are under the ion bombardment.

However, electric charges would buildup on the floating film whereas they would not buildup on the grounded film. Comparison of the plasma dewetting kinetics between floating and grounded metal films would single out the effect of charge buildup from the mixed effect. The plasma potential (Vp) is always higher than any electrodes or objects in the chamber. Since the potential of floating film (Vf) was 7 V, which is more positive than that of the grounded film, the H^+ ions are less accelerated toward the floating film than the grounded one. In other words, the bombardment effect of H^+ on the floating film should be diminished compared with that on the grounded film.

Besides, since figs. 3.2 - 3.5 show that the dewetting kinetics of the floating film is much higher than that of the grounded film, the results indicate that the enhanced kinetics of dewetting should come from the excess charge buildup from plasma. When the plasma discharge starts, both electrons and ions are abundantly generated. Since electrons are much more mobile than ions, a huge amount of electrons will be transferred to the grounded chamber wall. If the film is floating, however, electrons cannot flow easily to the ground. Therefore, an appreciable amount of excess electrons would buildup on the floating film whereas a much less amount would buildup on the grounded film.

The effect of excess charge buildup is further supported by fig. 3.6, where the elongated films are experiencing ion bombardment from the plasma regardless of the film location. However, the dewetting rate is relatively slow in fig. 3.6(b), where the conducting Al tape is nearby and therefore, excess electrons can easily pass through the conducting path to the substrate holder. As a result, excess electrons would have different residence time in each location of figs. 3.6(b), (c) and (d): the locations for figs. 3.6(b) and (d) would have respectively the shortest and the longest residence time of excess electrons. As a result, the amount of charge buildup would be much larger in fig. 3.6(d) than in fig. 3.6(b). Since the dewetting kinetics is much more enhanced in fig. 3.6(d) than in fig. 3.6(b), this result also supports that the charge buildup should enhance dewetting kinetics.

Applying bias is another way to build up electric charge on the film. Fig. 3.7 shows that applying bias of -8500 V is also effective in enhancing dewetting kinetics of the Sn film, additionally supporting the charge-enhanced dewetting kinetics. In fig. 3.7, it should be noted that the Sn film was heated to 300 ℃, which is ~ 70 ℃ above the melting point of Sn, which is 232 ℃. However, figs. 3.7(b) and (c) show that the Sn film did not melt. This means the Sn film was superheated. According to the literature survey, the film can be superheated when it is confined by other materials. For example, the compressed Pb layer sandwiched by Al films was superheated up to 120 ℃[83, 84]. Also, the compressed Pb epitaxial layer on Cu (111) melted 200 ℃ above the melting point[85]. In the case of fig. 3.7, the Sn film was confined between the Si substrate and the substrate holder. Superheating of the Sn film may be attributed to this confinement. As mentioned earlier, the possibility of superheating of

the Sn film was checked by putting a pure Sn granule together with the sample into the chamber. Then, the chamber was heated to 300 °C and maintained for 2 h. After the experiment, we checked the granule was melted while the dewetting of film did not occur. This result supports superheating of the Sn film.

It might be argued from the spherical shape of Sn particles in fig. 3.4(c) that the enhanced dewetting kinetics is attributed to melting of the Sn film, which is caused by ion bombardments from the plasma. In order to check this possibility, several Sn granules of 2 ~ 3 mm were placed on both floating and grounded substrates and were exposed to plasma at least for 2 min. On melting, the liquid drop would have a shape of a spherical cap on the substrate with the contact angle defined by the relative interfacial energies. However, the shape of Sn granules of 2 ~ 3 mm did not change at all, indicating that they did not melt. To check the change of temperature due to the plasma exposure, the temperature was measured by a thermocouple. The temperature varied slightly during the plasma exposure but was kept below 70 ℃ even after 2 min of plasma exposure.

The enhanced dewetting kinetics of Sn films would be achieved presumably by enhanced surface diffusion. This means that the charge buildup would enhance the surface diffusion. The enhanced kinetics by charge revealed in this paper might provide the important insight in the role of charge in non-classical crystallization, which helps understand how dense films without any voids or nanowires with smooth surface can grow by the building block of charged nanoparticles[68].

3.5 Conclusion

The dewetting kinetics was compared between floating and grounded Au films and Sn films on the Si substrate, respectively, which is exposed to inductively coupled plasma. The floating film had a much higher dewetting rate than the grounded one, indicating that the charge buildup enhances the dewetting kinetics. Also, the dewetting kinetics of the Sn film on elongated substrate, which had the conducting path made by an Al tape, increased with increasing distance from the conducting tape, indicating again that the charge buildup enhances the dewetting kinetics. The DC bias provided another way to induce the charge buildup, which was also shown to be effective in enhancing the dewetting kinetics. All these results not only indicate that the charge buildup enhances the dewetting kinetics of metal films but also imply that the charge buildup should generally enhance the kinetics other than dewetting.

Chapter 4.

4. Comparison of plasma effect on recrystallization kinetics of metal sheets between floating and grounded states

4.1 Introduction

There are increasing evidences that charges should make nanoparticles liquid-like or enhance diffusion in nanoparticles. To explain the void-free film or nanostructure growth by charged nanoparticles as building blocks, Hwang[68] suggested that charged nanoparticles should have a liquid-like property, which is attributed to weakening of the bond strength by charge[86]. More recently, Kim[87] compared the behavior of gold nanoparticles between grounded and floating states during in-situ TEM observations and confirmed that gold nanoparticles show liquid-like behavior only in the floating state. This result indicates that the liquid-like behavior of gold nanoparticles under electron irradiations does not come from the bombardments of high energy electrons but come from charges. In other words, charges make nanoparticles liquid-like or enhance diffusion kinetics.

Considering these, the well-known phenomenon of plasma enhanced kinetics should be reconsidered. Conventionally, plasma enhanced kinetics has been attributed to bombardments of high energy electrons or ions generated in the plasma[77, 88]. However, there is a possibility that the diffusion kinetics enhanced by plasma exposure should not come from electron or ion bombardments but come from

the charge buildup on the sample surface. The purpose of this study is to clarify whether the plasma enhanced kinetics should come from electron or ion bombardments or the charge buildup. In order to check whether plasma enhanced kinetics come from bombardments of ions or from the charge buildup, an experiment comparing recrystallization kinetics of the Fe-1%Si sheet sample in the inductively-coupled plasma between floating and grounded states was made. Also, an experiment comparing recrystallization kinetics of the pure Cu sheet sample in the inductively-coupled plasma between floating and grounded states was made.

4.2 Experimental details

In order to compare the plasma enhanced kinetics between floating and grounded samples, inductively coupled plasma (ICP) is used at the reactor pressure of 30 mtorr under flowing hydrogen (99.9999%) of 30 sccm. The plasma power was 650 W and 700 W. The schematic of the plasma reactor is shown in fig. 4.1. The two samples, one of which is made to be floating and the other of which is made to be grounded, are placed side by side and exposed to plasma simultaneously as shown in fig. 4.1. For the grounded sample, it is placed on the conducting stainless steel (SUS) substrate holder. For the floating sample, it is placed on the quartz crucible, which is placed on the substrate holder.

When the samples are exposed to plasma, their temperature is increased with time until it is saturated. For the plasma power of 700 W, the temperature of the samples is saturated at 300 ℃ after ~1 h.

For annealing experiment of Fe-1%Si steel, the samples needed to be heated separately because the recrystallization temperature of Fe-1%Si is around 650 ℃. For separate heating of the samples, the heating block was used inside the plasma chamber as shown in fig. 4.1. For temperature measurements of the sample, the thermocouple was used.

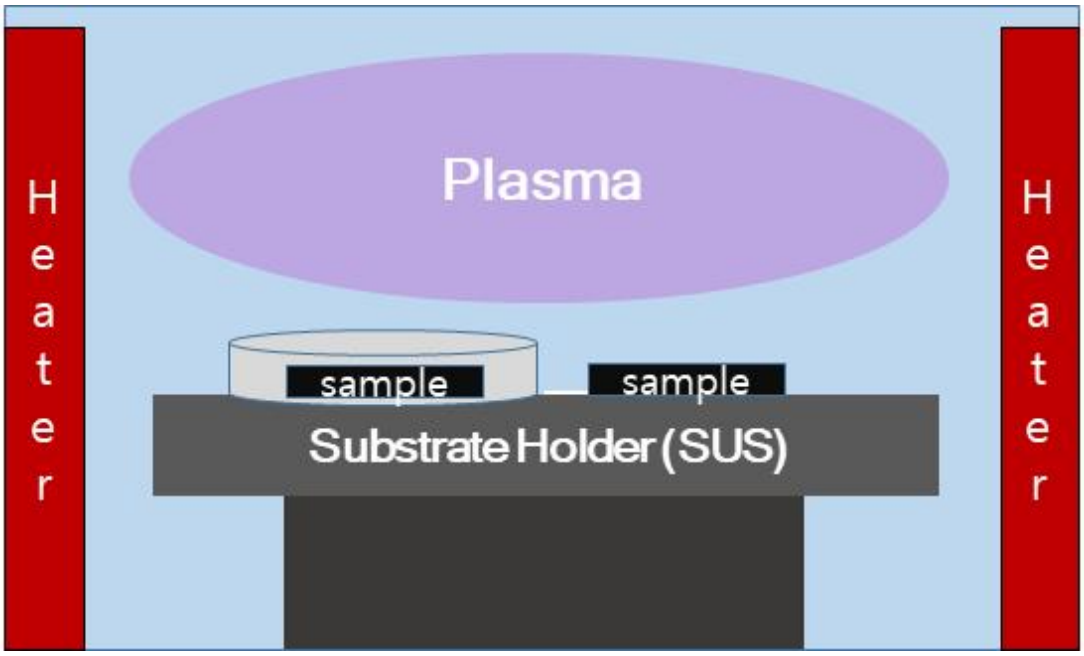

Fig. 4.1 Schematic of the inductively coupled plasma (ICP) chamber.

The cold-rolled sheet of Fe-1%Si (Fe-1%Si-0.054%Mn-0.005%P) which was 400 μm thick, was used. Each sample was cut to 10 mm × 10 mm. In order to see how much temperature is reduced for recrystallization of the cold-rolled Fe-1%Si sheet by plasma annealing, the sample heated solely by the heating block without plasma is necessary as a reference. For this reason, the cold-rolled Fe-1%Si sheet was heated by the heating block so that the thermocouple indicated 500 ℃ or 600 ℃, at the temperature of which the sample was annealed for 120 min in the absence of plasma. The recrystallization kinetics of these samples can be compared with that of the sample annealed in the presence of plasma. For this purpose, the sample was heated to 500 ℃ by the heating block, 10 min after which the sample was exposed to the ICP with the power of 700 W for 120 min. During the process, the temperature of the thermocouple tip was maintained at 500 ℃. The cross-section microstructure of the samples was compared by an optical microscope (OM) (AX10, ZEISS) after the surface was polished and etched with 2 % nital solution (98 % ethanol + 2 % nitric acid).

In order to identify the origin of the drastically increased recrystallization kinetics of the Fe-1%Si sheet by ICP, the temperature of the sample was decreased to 400 ℃ and the recrystallization kinetics was compared between floating and grounded samples while the samples were exposed to plasma with the power of 700 W for 120 min. Slightly different conditions were used to compare the recrystallization kinetics. The temperature of the sample was maintained at 450 ℃ after 10 min of which the ICP is turned with the power of 650 W for 120 min. In addition to observations of the polished sample surface by OM, the microstructure was analyzed

further by field emission scanning electron microscope (FESEM) (SU5000, HITACHI) or by electron back-scattered diffraction (EBSD) (TEL, HIKARI) attached to FESEM.

In order to check if the plasma effect is reproducible, recrystallization or grain growth kinetics of the cold-rolled sheet of Cu (99.5 %) was also compared between floating and grounded states. The starting material was a pure Cu ingot, which was hot rolled to 5 mm and followed by cold rolling to 400 μm. Each sample was cut to 10 mm × 10 mm. Then, the floating and grounded Cu sheets were placed side by side in the ICP chamber and exposed to plasma of 250 W for 120 min. In this case, the pure Cu sheet samples were heated only by plasma, not additionally heated by the heating block. Temperature of the thermocouple reached 160 °C after the experiment.

4.3 Results and discussion

The experimental result is shown in fig. 4.2, where the OM images of the polished surface are compared for the samples as-cold rolled (fig. 4.2(a)), thermally annealed at 600 °C (fig. 4.2(b)), thermally annealed at 500 °C (fig. 4.2(c)) and thermally and plasma annealed at 500 °C (fig. 4.2(d)). Figs. 4.2(b) and (c) show that recrystallization of the Fe-1%Si sheet hardly occurred after annealing for 120 min at 500 °C and 600 °C, not showing any noticeable change in the microstructure from that of the as-cold rolled sample (fig. 4.2(a)). However, the sample annealed at 500 °C in the presence of plasma with the power of 700 W shows the complete recrystallization as

shown in fig. 4.2(d). This result indicates that the plasma enhanced the recrystallization kinetics of the Fe-1%Si sheet. Fig. 4.2(d) is the image of the sample annealed in plasma under the floating condition. It should be noted that the image of the sample annealed in the plasma under the grounded condition is not much different from that of fig. 4.2(d).

Therefore, it is not clear whether the enhanced kinetics of recrystallization should come from electron bombardments or from the charge buildup. To clarify this, the kinetics should be compared between floating and grounded states under the condition that the recrystallization is only partly completed. For this purpose, the annealing temperature of the Fe-1%Si sheet sample is decreased to 400 °C and there crystallization kinetics was compared after 120 min of annealing between floating and grounded states with the plasma power of 700 W.

The result is shown in fig. 4.3. Recrystallization occurred in most area in the floating sample as shown in the OM image of fig. 4.3(a) and the EBSD image of fig. 4.3(b). In contrast, it hardly occurred in the grounded sample as shown in the OM image of fig. 4.3(c) and the EBSD image of fig. 4.3(d). When comparing fig. 4.3(e) with fig. 4.3(f), the average grain size of the floating sample is much larger than that of the grounded smaple. Fig. 4.3 clearly reveals that the recrystallization kinetics is much more enhanced by plasma in the floating sample than in the grounded one. This result indicates that the charge buildup rather than ion bombardment is responsible for the enhanced kinetics. If electron bombardments are responsible, the recrystallization kinetics should be enhanced much more on the

surface, which are bombarded by high energy electrons, than on the opposite side and the degree of recrystallization is decreased gradually toward the opposite side.

However, the microstructure characteristics in figs. 4.3(a) and (b) is far from that expected by electron bombardments. In figs. 4.3(a) and (b), the surface or its adjacent area, which is the top region of figs. 4.3(a) and (b), does not show any noticeable difference in recrystallization kinetics from the opposite side, which is the bottom area of figs. 4.3(a) and (b). The shear band, which appears horizontally along the rolling direction in figs. 4.3(a) and (b), represents the area where recrystallization is not completed. However, this shear band tends to be located in the upper middle area, not at the bottom area. This means that the recrystallization kinetics is faster in the bottom area than in the upper middle area. Considering that the chare buildup would occur at the surface in the conducting metal, the enhanced kinetics would be observed near the surface. This result also supports that the enhanced kinetics comes from the charge buildup.

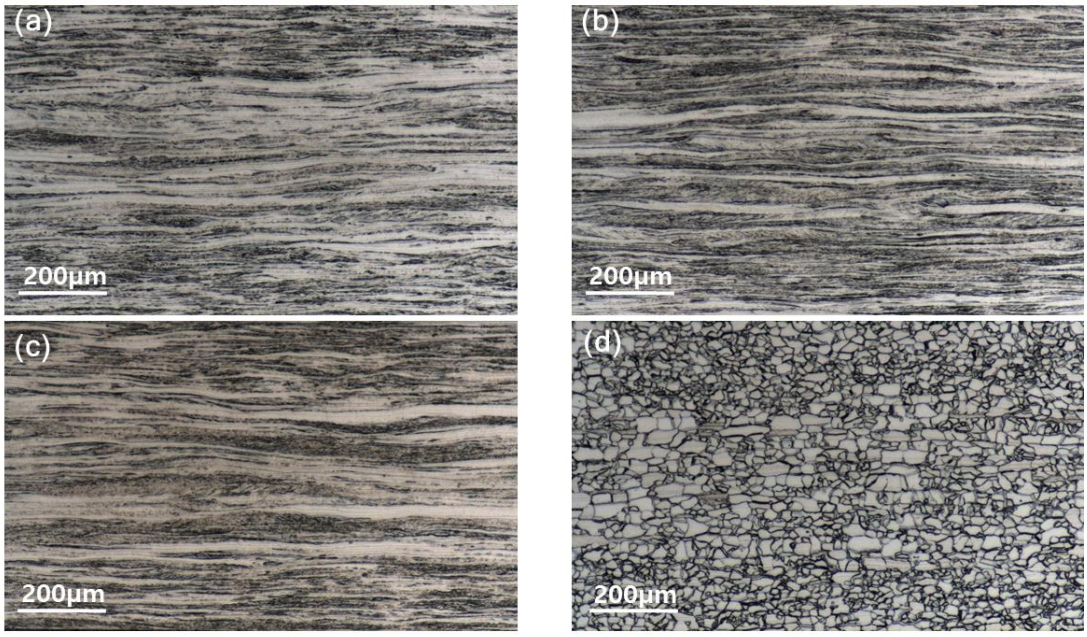

Fig. 4.2 OM cross section images of Fe-1%Si samples (a) as-cold rolled, (b) thermally annealed at 600 °C for 120 min, (c) thermally annealed 500 °C for 120 min and (d) thermally and plasma annealed at 500 °C for 120 min.

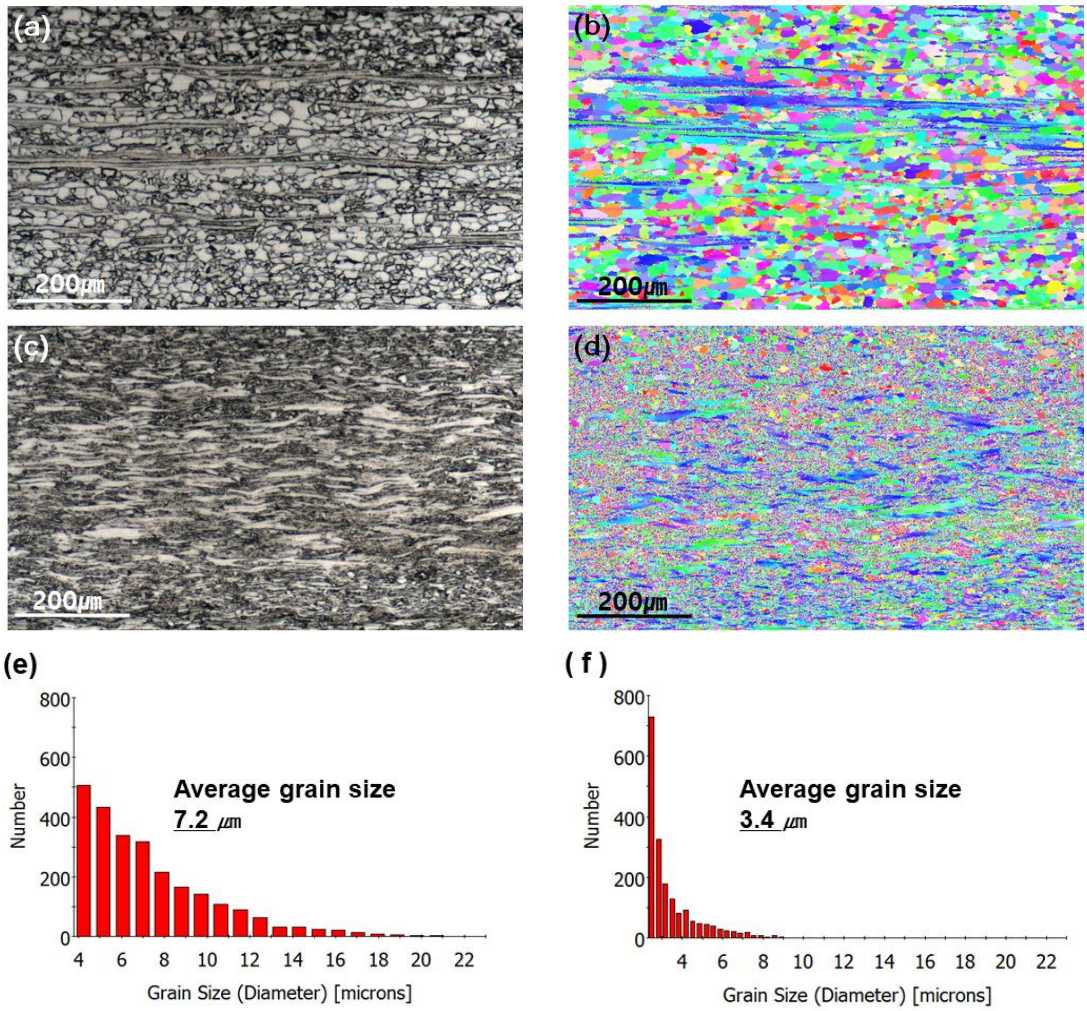

Fig. 4.3 (a) OM cross section and (b) EBSD images of floating Fe-1%Si sample heated for 120 min at 400 °C and exposed to plasma of 700 W, and (c) OM cross section and (d) EBSD images of grounded Fe-1%Si under the same condition. (e) Average grain size of the floating Fe-1%Si sample heated for 120 min at 400 °C and exposed to plasma of 700 W, and (f) Average grain size of grounded Fe-1%Si under the same condition.

Figs. 4.4(a) and (b) show the recrystallization fraction respectively of floating and grounded samples of fig. 4.3. The fraction of recrystallization was determined by calculating the grain orientation spread (GOS) value which is commonly used to evaluate the recrystallization fraction[89, 90]. The grains which have the 2° GOS value are regarded as recrystallized grains. The recrystallization fraction of figs. 4.4(a) and (b), which was calculated by the EBSD software, was respectively 0.77 and 0.20. Therefore, the recrystallization rate of the floating sample is much higher than that of the grounded one. Considering that the recrystallization hardly occurred at 600 ℃ for 120 min (fig. 4.2(b)) but was almost completed at 400 ℃ for 120 min when exposed to plasma of 700 W, it appears that the charge buildup by plasma could lower the recrystallization temperature at least by 200 °C.

The difference in recrystallization kinetics between floating and grounded samples was reproduced for the different temperature and plasma power. For example, figs. 4.5(a) and (b) show respectively OM cross section and EBSD images for the recrystallization fraction of Fe-1%Si heated at 450 °C and exposed to plasma of 650 W for 120 min in the floating state. Figs. 4.5(c) and (d) show respectively OM cross section and EBSD images for the recrystallization fraction of Fe-1%Si treated in the same condition as fig. 4.5(a) in the grounded state. Figs. 4.5(e) and (f) show respectively the average grain size of figs. 4.5(b) and (d). When fig. 4.5(a) is compared with fig. 4.5(c), it is clear that recrystallization kinetics of the floating sample is higher than that of the grounded sample. When comparing fig. 4.5(e) with fig. 4.5(f), the average grain size of the floating sample is much larger than that of the grounded sample. The

recrystallization fraction of fig. 4.5(b) and fig. 4.5(d) was respectively 0.45 and 0.18, again indicating that the recrystallization rate of the floating sample is much higher than that of the grounded one. Therefore, the enhanced recrystallization kinetics by the charge buildup is reproduced.

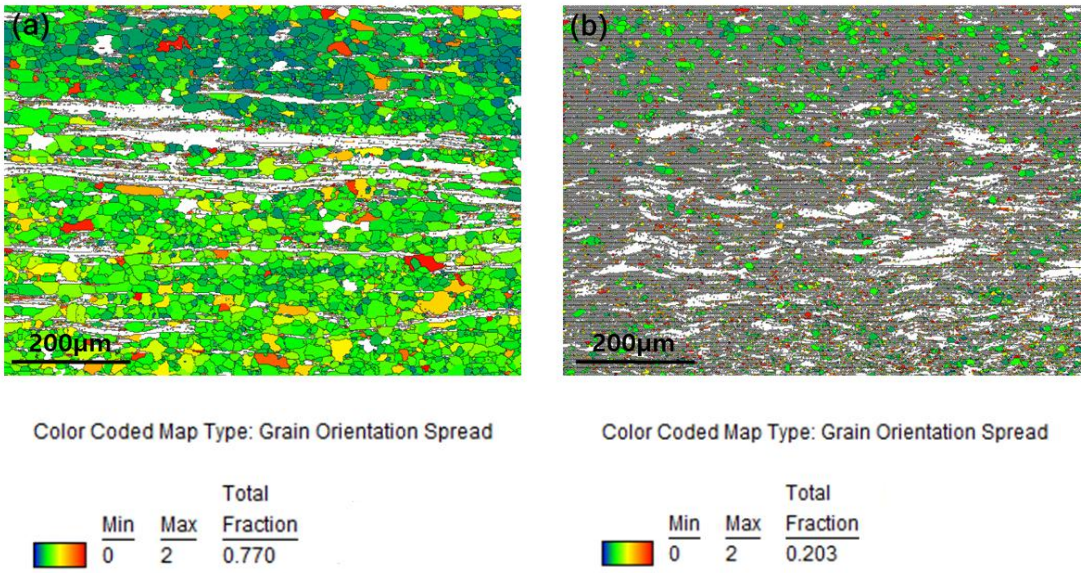

Fig. 4.4 EBSD images showing the recrystallization fraction of (a) floating and (b) grounded Fe-1%Si samples heated at 400 ℃ and exposed to plasma of 700 W.

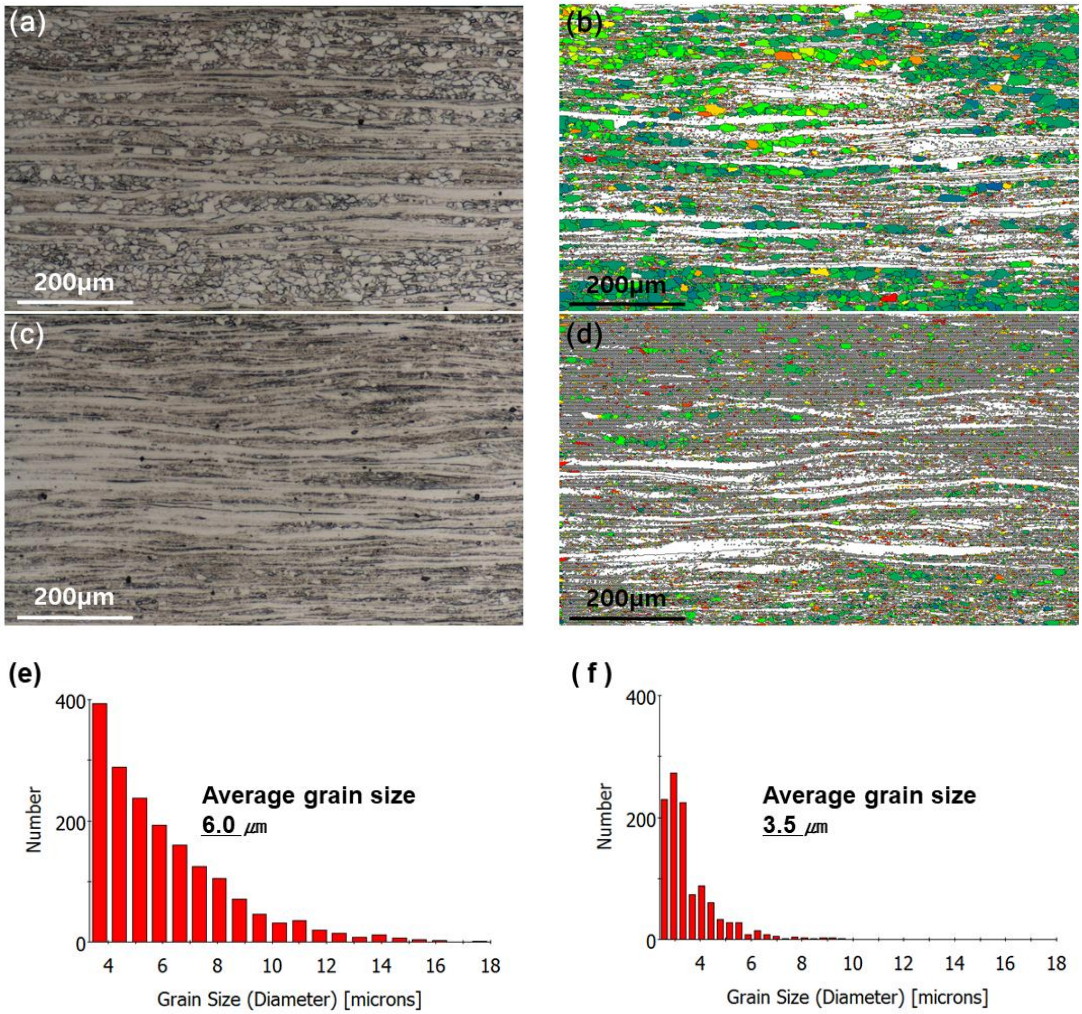

Fig. 4.5 (a) OM cross section and (b) EBSD images of floating Fe-1%Si sample heated for 120 min at 450 °C and exposed to plasma of 650 W and (c) OM cross section and (d) EBSD images of grounded Fe-1%Si sample heated for 120 min at 450 °C and exposed to plasma of 650 W. (e) Average grain size of the floating Fe-1%Si sample heated for 120 min at 450 °C and exposed to plasma of 650 W, and (f) Average grain size of the grounded Fe-1%Si under the same condition.

It is generally known that recovery, recrystallization and grain growth occur sequentially when cold-worked metals undergo annealing[91]. When comparing fig. 4.6(a) with fig. 4.6(b), both samples were fully recrystallized and grain growth occurred in both samples, but the difference in the grain size was remarkably large. This can be checked by comparing fig. 4.6(c) with fig. 4.6(d). The average grain size of the floating sample is much larger than that of the grounded sample. The grain growth is generally accompanied by the migration of the grain boundary. In an atomistic view, the rate of the grain boundary migration is proportional to the rate of atomic jumps across the grain boundary[92]. If the energy state of crystal defects of the grain boundary is excited by the excess charge buildup, the kinetic barrier for atomic jumps could be more easily overcome and the grain growth might be accelerated.

It should be reminded that the kinetics of dewetting and recrystallization enhanced by plasma would have been attributed to the bombardments of high energy electrons without the comparison of experiments between floating and grounded states. All the comparisons of kinetics between floating and grounded states indicate that the charge buildup enhances the kinetics of recrystallization of metal sheets as well as the kinetics of dewetting of films. Then, why does the charge enhance the kinetics? This is the on-going topics of our laboratory. Our preliminary study shows that the charge decreases the bond strength of molecules or bulks. For example, the bond strength of CH_4 is 5.9 eV. According to our ab-initio calculations, if CH_4 is negatively charged, the bond strength is decreased to 3.33 eV. And if it is positively charged, the bondstrength is decreased to 2.02 eV. When the nanoparticle is charged, the phonon vibration indicates its softening.

Plasma is used extensively in the industry. For example, if plasma is used in the CVD process, the precursor can be decomposed at lower temperature and crystalline films can be deposited at lower temperature. This is why the process is called plasma-enhanced CVD. Such enhanced kinetics has been attributed to the bombardments of high energy electron or the generation of the radicals. But our results imply the possibility that plasma can enhance the kinetics by providing electric charges. Our results also imply that the kinetic enhancement can be achieved not only by increasing the temperature but also by providing charges. Especially when the kinetic enhancement is required at low temperature, charge-enhanced kinetics can be a useful means.

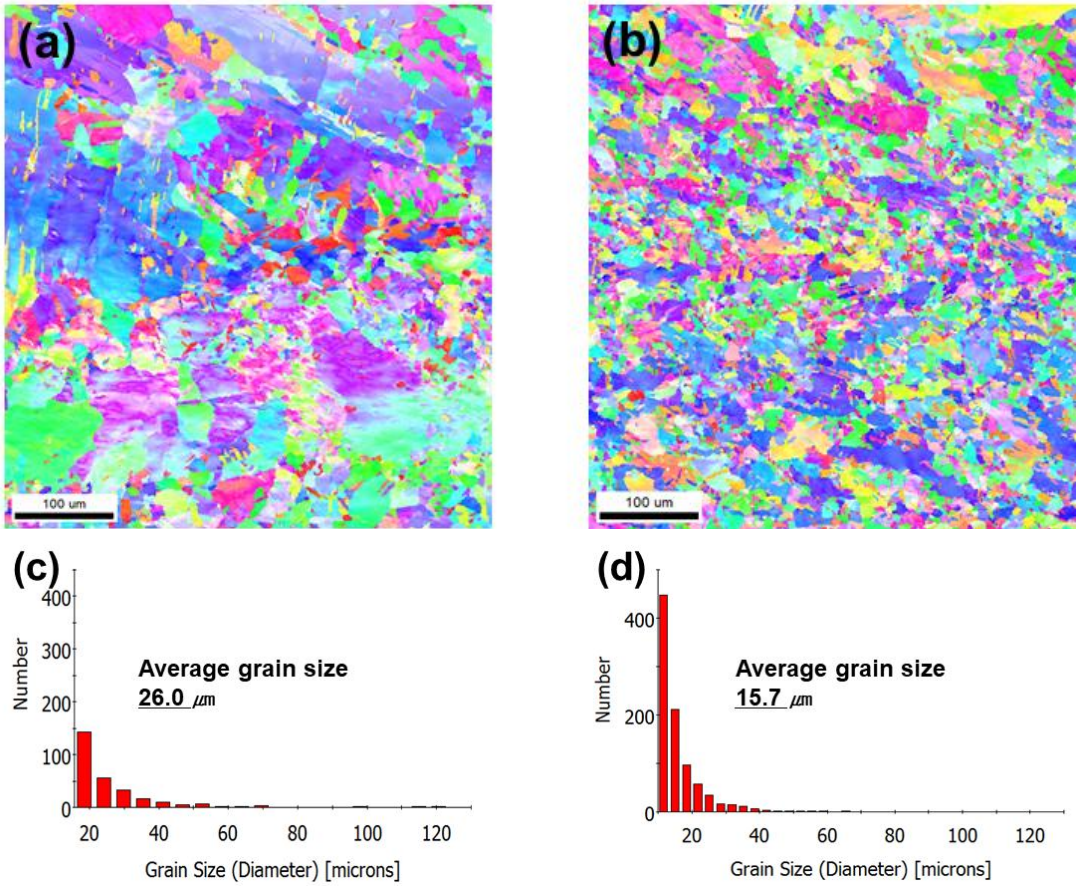

Fig. 4.6 EBSD images of (a) floating pure Cu sheet sample exposed to plasma of 250 W for 120 min, and (b) grounded pure Cu under the same condition. (c) Average grain size of floating pure Cu sheet sample exposed to plasma of 250 W for 120 min, and (d) Average grain size of grounded pure Cu under the same condition.

4.4 Conclusion

Comparison of recrystallization kinetics between floating and grounded states in the presence of plasma shows that the kinetics was enhanced much higher in the floating state than in the grounded state. The analysis of the result indicates that the charge buildup enhances the kinetics. This newly discovered concept of charge-enhanced kinetics can be used to enhance the kinetics in the material processing especially at low temperature.

References

[1] L. Boufendi, A. Plain, J.P. Blondeau, A. Bouchoule, C. Laure, M. Toogood, Measurements of particle size kinetics from nanometer to micrometer scale in a low-pressure argon-silane radio-frequency discharge, Applied physics letters, 60 (1992) 169-171.

[2] S. Vepřek, O. Ambacher, W. Rieger, K. Schopper, M. Vepřek-Heijman, Clusters in a silane glow discharge: Mechanism of their formation and how to avoid them, MRS Online Proceedings Library Archive, 297 (1993).

[3] M. Haverlag, W. Stoffels, E. Stoffels, G. Kroesen, F. De Hoog, Production and destruction of CF x radicals in radio-frequency fluorocarbon plasmas, Journal of Vacuum Science & Technology A: Vacuum, Surfaces, and Films, 14 (1996) 384-390.

[4] A. Garscadden, B. Ganguly, P. Haaland, J. Williams, Overview of growth and behaviour of clusters and particles in plasmas, Plasma Sources Science and Technology, 3 (1994) 239.

[5] N.M. Hwang, J.H. Hahn, D.Y. Yoon, Chemical potential of carbon in the low pressure synthesis of diamond, Journal of crystal growth, 160 (1996) 87-97.

[6] N.M. Hwang, J.H. Hahn, D.Y. Yoon, Charged cluster model in the low pressure synthesis of diamond, Journal of crystal growth, 162 (1996) 55-68.

[7] S.-W. Yoo, S.-J. You, J.-H. Kim, D.-J. Seong, B.-H. Seo, N.-M. Hwang, Effect of substrate bias on deposition behaviour of charged silicon nanoparticles in ICP-CVD process, Journal of Physics D: Applied Physics, 50 (2016) 035201.

[8] M. Niederberger, H. Cölfen, Oriented attachment and mesocrystals: non-classical crystallization mechanisms based on nanoparticle assembly, Physical chemistry chemical physics, 8 (2006) 3271-3287.

[9] H. Cölfen, M. Antonietti, Mesocrystals: inorganic superstructures made by highly parallel crystallization and controlled alignment, Angewandte Chemie International Edition, 44 (2005) 5576-5591.

[10] H. Cöelfen, M. Antonietti, Mesocrystals and nonclassical crystallization, John Wiley & Sons, 2008.

[11] E.R. Leite, C. Ribeiro, Crystallization and growth of colloidal nanocrystals, Springer Science & Business Media, 2011.

[12] R.L. Penn, J.F. Banfield, Imperfect oriented attachment: dislocation generation in defect-free nanocrystals, Science, 281 (1998) 969-971.

[13] N.M. Hwang, W.S. Cheong, D.Y. Yoon, Deposition behavior of Si on insulating and conducting substrates in the CVD process: approach by charged cluster model, Journal of crystal growth, 206 (1999) 177-186.

[14] N.M. Hwang, Deposition and simultaneous etching of Si in the chemical vapor deposition (CVD) process: approach by the charged

cluster model, Journal of crystal growth, 205 (1999) 59-63.

[15] N.M. Hwang, D.-Y. Kim, Low-pressure synthesis of diamond without hydrogen: approach by charged cluster model, Journal of crystal growth, 218 (2000) 40-44.

[16] N.M. Hwang, Evidence of nanometer-sized charged carbon clusters in the gas phase of the diamond chemical vapor deposition (CVD) process, Journal of crystal growth, 204 (1999) 85-90.

[17] N.M. Hwang, Crystal growth by charged cluster focused on CVD diamond process, Journal of crystal growth, 198 (1999) 945-950.

[18] N.M. Hwang, D.Y. Yoon, Thermodynamic approach to the paradox of diamond formation with simultaneous graphite etching in the low pressure synthesis of diamond, Journal of crystal growth, 160 (1996) 98-103.

[19] N.M. Hwang, W.S. Cheong, D.Y. Yoon, D.-Y. Kim, Growth of silicon nanowires by chemical vapor deposition: approach by charged cluster model, Journal of crystal growth, 218 (2000) 33-39.

[20] J.H. Hahn, N.M. Hwang, D.Y. Yoon, Formation of soot or diamond on the iron substrate in the chemical vapour deposition process of diamond, Journal of materials science letters, 15 (1996) 1240-1242.

[21] W.-K. Youn, S.-S. Lee, J.-Y. Lee, C.-S. Kim, N.-M. Hwang, S. Iijima, Comparison of the deposition behavior of charged silicon

nanoparticles between floating and grounded substrates, The Journal of Physical Chemistry C, 118 (2014) 11946-11953.

[22] W.-K. Youn, C.-S. Kim, N.-M. Hwang, Effect of the carrier gas flow rate on the microstructure evolution and the generation of the charged nanoparticles during silicon chemical vapor deposition, Journal of nanoscience and nanotechnology, 13 (2013) 7127-7130.

[23] N.-M. Hwang, D.-Y. Kim, Charged clusters in thin film growth, International materials reviews, 49 (2004) 171-190.

[24] P. Roca i Cabarrocas, Plasma enhanced chemical vapor deposition of amorphous, polymorphous and microcrystalline silicon films, J. Non-Cryst. Solids, 31 (2000) 266-269.

[25] S.V. Vladimirov, K. Ostrikov, Dynamic self-organization phenomena in complex ionized gas systems: new paradigms and technological aspects, Physics Reports, 393 (2004) 175-380.

[26] S. Nunomura, M. Kita, K. Koga, M. Shiratani, Y. Watanabe, In situ simple method for measuring size and density of nanoparticles in reactive plasmas, Journal of applied physics, 99 (2006) 083302.

[27] P.R. i Cabarrocas, N. Chaabane, A. Kharchenko, S. Tchakarov, Polymorphous silicon thin films produced in dusty plasmas: Application to solar cells, Plasma physics and controlled fusion, 46 (2004) B235.

[28] N. Chaâbane, V. Suendo, H. Vach, P. Roca i Cabarrocas, Soft

landing of silicon nanocrystals in plasma enhanced chemical vapor deposition, Applied physics letters, 88 (2006) 203111.

[29] A.F. i Morral, P.R. i Cabarrocas, Etching and hydrogen diffusion mechanisms during a hydrogen plasma treatment of silicon thin films, Journal of non-crystalline solids, 299 (2002) 196-200.

[30] P.R. i Cabarrocas, Plasma enhanced chemical vapor deposition of silicon thin films for large area electronics, Current Opinion in Solid State and Materials Science, 6 (2002) 439-444.

[31] K. Ostrikov, A. Murphy, Plasma-aided nanofabrication: where is the cutting edge?, Journal of Physics D: Applied Physics, 40 (2007) 2223.

[32] K. Ostrikov, E. Neyts, M. Meyyappan, Plasma nanoscience: from nano-solids in plasmas to nano-plasmas in solids, Advances in Physics, 62 (2013) 113-224.

[33] K. Ostrikov, S. Xu, S. Huang, I. Levchenko, Nanoscale surface and interface engineering: Why plasma-aided?, Surface and Coatings Technology, 202 (2008) 5314-5318.

[34] K. Ostrikov, M. Yu, L. Stenflo, Surface waves in strongly irradiated dusty plasmas, Physical Review E, 61 (2000) 782.

[35] K. Koga, T. Inoue, K. Bando, S. Iwashita, M. Shiratani, Y. Watanabe, Highly stable a-Si: H films deposited by using multi-hollow plasma chemical vapor deposition, Japanese journal of applied

physics, 44 (2005) L1430.

[36] M. Shiratani, H. Kawasaki, T. Fukuzawa, H. Tsuruoka, T. Yoshioka, Y. Watanabe, Study on growth processes of particulates in helium-diluted silane rf plasmas using scanning electron microscopy, Applied physics letters, 65 (1994) 1900-1902.

[37] Y. Watanabe, Formation and behaviour of nano/micro-particles in low pressure plasmas, Journal of Physics D: Applied Physics, 39 (2006) R329.

[38] E. Persidis, H. Baur, F. Pieralisi, P. Schalberger, N. Fruehauf, Area laser crystallized LTPS TFTs with implanted contacts for active matrix OLED displays, Solid-State Electronics, 52 (2008) 455-461.

[39] S. Uchikoga, N. Ibaraki, Low temperature poly-Si TFT-LCD by excimer laser anneal, Thin Solid Films, 383 (2001) 19-24.

[40] A. Shah, P. Torres, R. Tscharner, N. Wyrsch, H. Keppner, Photovoltaic technology: the case for thin-film solar cells, science, 285 (1999) 692-698.

[41] H. Kahn, N. Tayebi, R. Ballarini, R. Mullen, A. Heuer, Fracture toughness of polysilicon MEMS devices, Sensors and Actuators A: Physical, 82 (2000) 274-280.

[42] K. Wang, H. Hwang, P. Leong, T. Yew, Microstructures of low-temperature-deposited polycrystalline silicon with micrometer grains, Journal of applied physics, 77 (1995) 6542-6548.

[43] H.S. Tae, S.H. Hwang, S.J. Park, E. Yoon, K.W. Whang, Effects of process parameters on low-temperature silicon homoepitaxy by ultrahigh-vacuum electron-cyclotron-resonance chemical-vapor deposition, Journal of applied physics, 78 (1995) 4112-4117.

[44] H.S. Tae, S.J. Park, S.H. Hwang, K.H. Hwang, E. Yoon, K.W. Whang, S.A. Song, Low-temperature in situ cleaning of silicon (100) surface by electron cyclotron resonance hydrogen plasma, Journal of Vacuum Science & Technology B: Microelectronics and Nanometer Structures Processing, Measurement, and Phenomena, 13 (1995) 908-913.

[45] A. Asano, Effects of hydrogen atoms on the network structure of hydrogenated amorphous and microcrystalline silicon thin films, Applied physics letters, 56 (1990) 533-535.

[46] R. Nozawa, H. Takeda, M. Ito, M. Hori, T. Goto, Substrate bias effects on low temperature polycrystalline silicon formation using electron cyclotron resonance SiH 4/H 2 plasma, Journal of applied physics, 81 (1997) 8035-8039.

[47] J. Schwarzkopf, B. Selle, W. Bohne, J. Röhrich, I. Sieber, W. Fuhs, Disorder in silicon films grown epitaxially at low temperature, Journal of applied physics, 93 (2003) 5215-5221.

[48] J.P. Van Der Eerden, Handbook of Crystal Growth Vol. 1a: Bulk Fundamentals, Growth Thermodynamics and Kinetics, North-Holland, Amsterdam, 1994.

[49] G.G.H. Bennema P, Crystal Growth: An Introduction Wiley, Newyork, USA, 1973.

[50] J.H. Hahn, N.M. Hwang, D.Y. Yoon, Formation of soot or diamond on the iron substrate in the chemical vapour deposition process of diamond, Journal of materials science letters, 15 (1996) 1240-1242.

[51] A. Howling, L. Sansonnens, J.-L. Dorier, C. Hollenstein, Negative hydrogenated silicon ion clusters as particle precursors in RF silane plasma deposition experiments, Journal of Physics D: Applied Physics, 26 (1993) 1003.

[52] S. Veprek, O. Ambacher, W. Rieger, K. Schopper, M.G.J. Veprek-Heijman, Clusters in a silane glow discharge: Mechanism of their formation and how to avoid them, Materials Research Society Symposium Proceedings, 1993, pp. 13-18.

[53] A. Garscadden, B. Ganguly, P. Haaland, J. Williams, Overview of growth and behaviour of clusters and particles in plasmas, Plasma Sources Science and Technology, 3 (1994) 239.

[54] E. Stoffels, W. Stoffels, G. Kroesen, F. De Hoog, Dust formation and charging in an Ar/SiH4 radio-frequency discharge, Journal of Vacuum Science & Technology A: Vacuum, Surfaces, and Films, 14 (1996) 556-561.

[55] N.-M. Hwang, D.-K. Lee, Charged nanoparticles in thin film and nanostructure growth by chemical vapour deposition, Journal of

Physics D: Applied Physics, 43 (2010) 483001.

[56] M.A. Lieberman, A.J. Lichtenberg, Principles of plasma discharges and materials processing, John Wiley & Sons, 2005.

[57] A. Melzer, T. Trottenberg, A. Piel, Experimental determination of the charge on dust particles forming Coulomb lattices, Physics Letters A, 191 (1994) 301-308.

[58] T. Trottenberg, A. Melzer, A. Piel, Measurement of the electric charge on particulates forming Coulomb crystals in the sheath of a radiofrequency plasma, Plasma Sources Science and Technology, 4 (1995) 450.

[59] U. Kortshagen, G. Mümken, The electrical charging of micron-sized dust particles in a capacitively coupled RF plasma, Physics Letters A, 217 (1996) 126-132.

[60] T. Matsoukas, M. Russell, M. Smith, Stochastic charge fluctuations in dusty plasmas, Journal of Vacuum Science & Technology A: Vacuum, Surfaces, and Films, 14 (1996) 624-630.

[61] K.-S. Kim, D.-J. Kim, J.-H. Yoon, J.Y. Park, Y. Watanabe, M. Shiratani, The changes in particle charge distribution during rapid growth of particles in the plasma reactor, Journal of colloid and interface science, 257 (2003) 195-207.

[62] M. Shiratani, H. Kawasaki, T. Fukuzawa, T. Yoshioka, Y. Ueda, S. Singh, Y. Watanabe, Simultaneous in situ measurements of properties

of particulates in rf silane plasmas using a polarization-sensitive laser-light-scattering method, Journal of applied physics, 79 (1996) 104-109.

[63] P.R. i Cabarrocas, T. Nguyen-Tran, Y. Djeridane, A. Abramov, E. Johnson, G. Patriarche, Synthesis of silicon nanocrystals in silane plasmas for nanoelectronics and large area electronic devices, Journal of Physics D: Applied Physics, 40 (2007) 2258.

[64] S.W. Yoo, S.J. You, J.H. Kim, D.J. Seong, B.H. Seo, N.M. Hwang, Effect of substrate bias on deposition behaviour of charged silicon nanoparticles in ICP-CVD process, J Phys D Appl Phys, 50 (2017) 035201.

[65] J.K. Rath, B. Stannowski, P.A. van Veenendaal, M.K. van Veen, R.E. Schropp, Application of hot-wire chemical vapor-deposited Si: H films in thin film transistors and solar cells, Thin Solid Films, 395 (2001) 320-329.

[66] A. Shah, J. Meier, E. Vallat-Sauvain, N. Wyrsch, U. Kroll, C. Droz, U. Graf, Material and solar cell research in microcrystalline silicon, Solar Energy Materials and Solar Cells, 78 (2003) 469-491.

[67] T.Y. Takagi, I.; Sasaki, A., Film formation by ionised-cluster beam deposition, in: J.L. A. Moruzzi (Ed.) Film formation by ionised-cluster beam deposition, Institute of Physics, United Kingdom, 1977.

[68] N.M. Hwang, Non-Classical Crystallization of Thin Films and Nanostructures in CVD and PVD Processes, Springer, USA, 2016.

[69] S. Iijima, T. Ichihashi, Structural instability of ultrafine particles of metals, Physical review letters, 56 (1986) 616.

[70] J.-S. Jung, S.-H. Lee, D.-S. Kim, K.-S. Kim, S.-W. Park, N.-M. Hwang, Non-classical crystallization of silicon thin films during hot wire chemical vapor deposition, Journal of Crystal Growth, 458 (2017) 8-15.

[71] J. Schulze, E. Schüngel, U. Czarnetzki, The electrical asymmetry effect in capacitively coupled radio frequency discharges–measurements of dc self bias, ion energy and ion flux, Journal of Physics D: Applied Physics, 42 (2009) 092005.

[72] H. Yokoyama, M. Okamoto, Y. Osaka, Effects of a negative self-bias on the growth of cubic boron nitride prepared by plasma chemical vapor deposition, Japanese journal of applied physics, 30 (1991) 344.

[73] C.V. Thompson, Solid-State Dewetting of Thin Films, Annu Rev Mater Res, 42 (2012) 399-434.

[74] F. Niekiel, P. Schweizer, S.M. Kraschewski, B. Butz, E. Spiecker, The process of solid-state dewetting of Au thin films studied by in situ scanning transmission electron microscopy, Acta Materialia, 90 (2015) 118-132.

[75] J.-Y. Kwon, T.-S. Yoon, K.-B. Kim, S.-H. Min, Comparison of the agglomeration behavior of Au and Cu films sputter deposited on silicon dioxide, Journal of applied physics, 93 (2003) 3270-3278.

[76] K. Sieradzki, K. Bailey, T. Alford, Agglomeration and percolation conductivity, Applied Physics Letters, 79 (2001) 3401-3403.

[77] S.-H. Kwon, H.J. Choe, H.-C. Lee, C.-W. Chung, J.-J. Lee, Mechanism of solid-state plasma-induced dewetting for formation of copper and gold nanoparticles, Journal of nanoscience and nanotechnology, 13 (2013) 6109-6114.

[78] H. Choe, S.-H. Kwon, C. Choe, J.-J. Lee, C.-H. Woo, Sn microparticles made by plasma-induced dewetting, Thin Solid Films, 620 (2016) 165-169.

[79] S. Iijima, Some experiments on structural instability of small particles of metals, Microclusters, Springer, 1987, pp. 186-199.

[80] K. Kim, Analysis of Dynamic Behavior of Metal Nano-particles with Different Conductivity of Substrate using In-situ TEM : The Effect of Charge, Seoul National University, Seoul, 2018.

[81] S.-H. Kwon, D.-H. Han, H.J. Choe, J.-J. Lee, Synthesis of copper nanoparticles by solid-state plasma-induced dewetting, Nanotechnology, 22 (2011) 245608.

[82] F. Leroy, F. Cheynis, Y. Almadori, S. Curiotto, M. Trautmann, J. Barbe, P. Müller, How to control solid state dewetting: A short review, Surface Science Reports, 71 (2016) 391-409.

[83] L. Zhang, Z. Jin, L. Zhang, M. Sui, K.J.P.r.l. Lu, Superheating of confined Pb thin films, 85 (2000) 1484.

[84] J. Akhter, Z. Jin, K.J.J.o.P.C.M. Lu, Superheating in confined Pb (110) films, 13 (2001) 7969.

[85] G. Meyer, M. Michailov, M.J.S.S. Henzler, LEED studies of the epitaxy of Pb on Cu (111), 202 (1988) 125-141.

[86] B.W. Clare, G. Talukder, P.J. Jennings, J.C.L. Cornish, G.T. Hefter, Effect of charge on bond strength in hydrogenated amorphous silicon, Journal of computational chemistry, 15 (1994) 644-652.

[87] K. Kim, Analysis of Dynamic Behavior of Metal Nano-particles with Different Conductivity of Substrate using In-situ TEM: The Effect of Charge, Seoul National University, 2018.

[88] E.I. Meletis, Intensified plasma-assisted processing: science and engineering, Surface and Coatings Technology, 149 (2002) 95-113.

[89] D. Field, L. Bradford, M. Nowell, T. Lillo, The role of annealing twins during recrystallization of Cu, Acta materialia, 55 (2007) 4233-4241.

[90] R.J. Mccabe, D.F. Teter, Analysis of recrystallized volume fractions in uranium using electron backscatter diffraction, Journal of microscopy, 223 (2006) 33-39.

[91] R. Abbaschian, R.E. Reed-Hill, Physical metallurgy principles, Cengage Learning, 2008.

[92] D.A. Porter, K.E. Easterling, M. Sherif, Phase Transformations in

Metals and Alloys, (Revised Reprint), CRC press, 2009.

요약(국문초록)

하전이 나노입자를 마치 액체처럼 거동하게 하거나(liquid-like) 나노입자의 확산을 증가시킨다는 증거들이 점점 많이 제시되고 있다. 이를 고려하여, 박막증착의 기본단위를 기상에서 생성되는 하전된 나노입자라고 주장하는 비고전적 결정성장이론을 이용하여 RF-PECVD 시스템에서 실리콘 박막증착 거동에 관한 연구를 진행하였다.

에피택셜 박막증착에 미치는 기판 바이어스의 영향을 알아보기 위해, 기판홀더에 각각 0 V, +1000 V 그리고 -1000 V 를 가해주고 실리콘기판을 이용하여 박막증착 실험을 진행하였다. 온도조건 550 ℃ 하에서 기판에 바이어스를 걸어주지 않은 조건에서는 대부분 비정질의 실리콘 박막이 증착된 반면, 온도조건 550 ℃ 하에서 기판에 -1000 V 를 가해주었을 때에는 완전한 에피택셜 박막이 증착되었다. 그리고 RF-PECVD 챔버에서 나노입자의 존재를 확인하기 위해, 기판홀더위에 TEM 그리드를 올려놓고 DC바이어스를 걸어준 다음 나노입자 포집실험을 진행하였다. 이를 통해 기판에 가해주는 바이어스와 멤브레인의 전도도에 따라 나노입자의 포집 거동이 달라짐을 확인하였다.

또한, 플라즈마로 인한 키네틱의 증가가 이온의 봄바드먼트 때문인지 하전으로 인한 것인지 확인하기 위해, 두 종류의 실험을 진행하였다. 먼저 ICP 장비에서 금 박막과 주석 박막을 이용하여 전기적으로 플로팅상태와 그라운드상태에 따른 디웨팅 키네틱을 비교하였다. 그리고 Fe-1%Si 과 순수 구리시편을 이용하여 플로팅상태와 그라운드상태에 따른 재결정거동을 비교하였다. 디웨팅과 재결정 모두 그라운드상태일 때 보다 플로팅상태일 때 키네틱이 훨씬 크게 증가하는 것을 알 수 있었다. 이는 하전의 쌓임이 플라즈마로 인한 키네틱 증가에 절대적인 영향을 끼친 것임을 의미한다.

주요어 : 비고전적 결정화; 하전; 실리콘; 에피택셜 박막증착; 디웨팅; 재결정;

학 번 : 2014 - 22517